Journal of Computational Physics 442 (2021) 110496

Contents lists available at ScienceDirect

Journal of Computational Physics

www.elsevier.com/locate/jcp

Unified gas-kinetic wave-particle methods V: Diatomic molecular flow

Xiaocong Xu [a], Yipei Chen [a], Chang Liu [a], Zhihui Li [b], Kun Xu [a,c,*]

[a] Department of Mathematics, Hong Kong University of Science and Technology, Hong Kong
[b] National Laboratory for Computational Fluid Dynamics, Beijing University of Aeronautics and Astronautics, Beijing 100191, China
[c] Shenzhen Research Institute, Hong Kong University of Science and Technology, Shenzhen, China

ARTICLE INFO

Article history:
Available online 10 June 2021

Keywords:
Unified gas-kinetic wave-particle method
Multiscale transport
Diatomic gas
Hypersonic non-equilibrium flow

ABSTRACT

In this paper, the unified gas-kinetic wave-particle (UGKWP) method is further developed for diatomic gas with the energy exchange between translational and rotational modes for flow study in all regimes. The multiscale transport mechanism in UGKWP is coming from the direct modelling in a discretized space, where the cell's Knudsen number, defined by the ratio of particle mean free path over the numerical cell size, determines the flow physics simulated by the wave particle method. The non-equilibrium distribution function in UGKWP is tracked by the discrete particle and analytical wave. The weights of distributed particle and wave in different regimes depend on cell's Knudsen number, where distinguishable macroscopic flow variables of particle and wave are updated inside each control volume. The UGKWP becomes a particle method in the highly rarefied flow regime and converges to the gas-kinetic scheme (GKS) for the Navier-Stokes solution in the continuum flow regime without particles. In comparison with discrete velocity method (DVM)-based unified gas-kinetic scheme (UGKS), the computational cost and memory requirement in UGKWP have been reduced by several orders of magnitude for the high speed and high temperature flow simulation, where the translational and rotational non-equilibrium can be captured accurately in the transition and rarefied regime. As a result, for the hypersonic flow around a flying vehicle, the computation can be conducted using a personal computer for the studies in all regimes. The UGKWP method for diatomic gas will be validated in various cases from one dimensional shock structure to three dimensional flow over a sphere, and the numerical solutions will be compared with the reference DSMC results and experimental measurements.

1. Introduction

Kinetic equations describe the gas flow by modelling the evolution of the gas probability density function (PDF) through particle transport and collision. The Boltzmann equation is constructed on the particle mean free path and mean collision time scale. In order to simplify the collisional operator of the Boltzmann equation, many relaxation models, such as the Bhatnagar-Gross-Krook (BGK) model [1], the ellipsoidal statistical BGK (ES-BGK) model [2], and the Shakhov BGK (S-BGK) model [3], have been developed and used in theoretical analysis and engineering applications. Theoretically, these kinetic

* Corresponding author at: Department of Mathematics, Hong Kong University of Science and Technology, Hong Kong.
E-mail addresses: xxuay@connect.ust.hk (X. Xu), ychendh@connect.ust.hk (Y. Chen), cliuaa@connect.ust.hk (C. Liu), zhli0097@x263.net (Z. Li), makxu@ust.hk (K. Xu).

https://doi.org/10.1016/j.jcp.2021.110496
0021-9991/

equations are valid in all flow regimes, but with a resolved dynamics on the kinetic scale. The numerical methods for solving kinetic equations can be classified into the stochastic methods and the deterministic methods.

For the stochastic methods, the discrete particles are employed to simulate the evolution of the PDF. This kind of Lagrangian-type scheme can easily keep the positivity and conservation properties with super stability. The direct simulation Monte Carlo (DSMC) method [4] is one of the most representative stochastic methods. By modelling the particle transport and collision separately, DSMC achieves great success in the simulation of high speed and rarefied non-equilibrium gas flow. However, the DSMC method will suffer from the statistical noise in the low speed flow simulation. Meanwhile, due to the splitting treatment of particle transport and collision, the cell size and time step are restricted to be less than the particle mean free path and collision time. Under this circumstance, the computational cost for the near continuum flow will increase rapidly. For the deterministic approaches, the most popular methods are the so-called discrete velocity method (DVM) for the Boltzmann and kinetic equations [5–13]. When the Knudsen number is small, the collision operator in the kinetic equation becomes stiff, which will strongly restrict the time step. To improve the computational efficiency, the asymptotic preserving (AP) schemes have been proposed and developed [14]. Based on the DVM framework, many kinetic solvers have been developed for diatomic gas as well [15,16].

Following the direct modelling methodology [17], an effective multiscale unified gas-kinetic scheme (UGKS) has been proposed for both monatomic and diatomic gases for the flow study in all regimes [11,18–21]. Under the UGKS framework, the numerical flux is constructed from the integral solution of the kinetic model equation, where the effect of particle transport and collision is accumulated in a time step to identify the flow regime. The UGKS has an asymptotic limit to the Navier-Stokes (NS) equations in the continuum flow regime without kinetic scale restriction on time step and cell size, which has the so-called unified preserving (UP) property [22]. Moreover, the implicit and multi-grid techniques have also been incorporated into the UGKS [23–25] to improve the computational efficiency. Recently, the unified gas-kinetic wave-particle (UGKWP) method [26,27] based on the BGK model has been developed for monatomic gas. The essential idea of UGKWP is to use stochastic particles and wave together to replace the discretization of particle velocity space. In UGKWP, the gas particles are divided into hydro-particle, collisional particle, and collisionless particle. The hydro-particle is described by the analytic PDF, while the collisional and collisionless particles are described by the simulation particles. In UGKWP, the macroscopic flow variables will be updated under the finite volume framework, where both analytical PDF and simulating particles will contribute to the cell interface flux. One of the distinguishable features of UGKWP is that the dynamic evolution of hydro-particle can be described analytically and the computational cost for capturing the hydro-particles is comparable to a hydrodynamic solver. The proportion of three kinds of particles varies dynamically in different flow regimes. Physically, the collisionless particles are mainly used for the description of non-equilibrium transport and the hydro-particles for the equilibrium one. The dynamic evolution among three kinds of particles is coupled with the variation of cell's Knudsen number. In the continuum flow regime, the number of collisional and collisionless particles will be greatly reduced and the UGKWP method automatically converges to the gas-kinetic scheme (GKS) for the Navier-Stokes solutions [28], which has the similar efficiency as a conventional NS solver. For the simulation of hypersonic flow, the UGKWP method will be much more efficient than the original DVM-based UGKS due to the use of simulation particles instead of discretizing the particle velocity space. In summary, the computational cost of the UGKWP method is similar to the particle method in rarefied regime and becomes the hydrodynamic flow solver in continuum regime. The UGKWP is also extended to other multiscale transport, such as radiation and plasma [29,30].

This paper is about the development of the UGKWP method for diatomic gas, where the Rykov kinetic model will be used in the construction of the evolution solution of the gas distribution function, which controls the distribution of particle and wave and the rate of energy exchange between translational and rotational degrees of freedom. A simple and efficient way to set up the correct transport coefficients is presented in this paper. A weighted method is applied to sample the particles from a modified distribution function of the Rykov model. The overall UGKWP method for diatomic gas is very efficient and has excellent performance for high speed flow simulation with the translational and rotational non-equilibrium.

The rest of the paper is organised as follows. In Section 2, the unified gas-kinetic particle method (UGKP) for diatomic gas will be introduced first. Then, based on the analytical formulation of the hydro-particle, the unified gas-kinetic wave-particle method will be presented, which is an improved version of the UGKP. The asymptotic preserving property of the UGKWP method for diatomic gas in the continuum regime will be introduced in section 3. Section 4 includes various numerical tests to validate the new scheme. Section 5 is the conclusion.

2. Unified gas-kinetic wave-particle method for diatomic gas

2.1. The Rykov kinetic model for diatomic gas

Diatomic gas is associated with translational, rotational, and vibrational modes. For relatively low temperature flow, there are two rotational degrees of freedom while the vibrational modes get basically frozen. In this paper, the diatomic gas with translational and rotational degrees of freedom will be considered. For nitrogen gas, the molecule has three translational degrees of freedom and two rotational ones. The state of the gas can be described by the particle velocity distribution function $f(\vec{x}, t, \vec{v}, \vec{\xi})$, where $\vec{x}$ is the spatial coordinate, t is the time, $\vec{v}$ is the molecular translational velocity, and $\vec{\xi}$ is the rotational variable. The relations between distribution function and macro-variables are defined as

$$\vec{W} = \int \vec{\psi} f d\Xi,$$

with $d\Xi = d\vec{v}d\vec{\xi}$, where $\vec{\psi} = \left(1, \vec{v}, \frac{1}{2}(\vec{v}^2 + \vec{\xi}^2), \frac{1}{2}\vec{\xi}^2\right)$ is the vector for the moments of distribution function and $\vec{W} = (\rho, \rho\vec{U}, \rho E, \rho E_{rot})$ is the macroscopic variables with ρE_{rot} as the rotational energy density. The stress tensor $\mathbf{P}$ and the heat fluxes $\vec{q}_t$ and $\vec{q}_r$ produced by the transfer of translational and rotational energies, can be calculated by f as,

$$\begin{aligned}
\mathbf{P} &= \int \vec{c}\vec{c} f d\Xi, \\
\vec{q}_t &= \frac{1}{2}\int \vec{c}\vec{c}^2 f d\Xi, \\
\vec{q}_r &= \frac{1}{2}\int \vec{c}\vec{\xi}^2 f d\Xi,
\end{aligned}$$

where $\vec{c} = \vec{v} - \vec{U}$ is the peculiar velocity. The total heat flux $\vec{q}$ is the sum of $\vec{q}_t$ and $\vec{q}_r$, such as

$$\vec{q} = \frac{1}{2}\int \vec{c}\left(\vec{c}^2 + \vec{\xi}^2\right) f d\Xi = \vec{q}_t + \vec{q}_r.$$

The evolution of the diatomic gas distribution function f is governed by the Rykov kinetic model equation,

$$\frac{\partial f}{\partial t} + \vec{v}\cdot\nabla_{\vec{x}} f = \frac{\tilde{M}_t - f}{\tau} + \frac{\tilde{M}_{eq} - \tilde{M}_t}{Z_{rot}\tau}, \tag{1}$$

where the collision operator on the right-hand side describes the elastic and inelastic collisions. The elastic collision conserves the translational energy, while the inelastic collision exchanges the translational and rotational energy. $\tilde{M}_t$ is the modified equilibrium distribution function for the elastic collision while $\tilde{M}_{eq}$ is the modified equilibrium state for inelastic collision, which are expressed as,

$$\begin{aligned}
\tilde{M}_t &= M_t + M_t^+, \\
M_t &= \rho\left(\frac{\lambda_t}{\pi}\right)^{\frac{3}{2}} e^{-\lambda_t\vec{c}^2}\frac{\lambda_r}{\pi}e^{-\lambda_r\vec{\xi}^2}, \\
M_t^+ &= M_t\left(\frac{4\lambda_t^2\vec{q}_t\cdot\vec{c}}{15\rho}\left(2\lambda_t\vec{c}^2 - 5\right) + \frac{4(1-\sigma)\lambda_t\lambda_r\vec{q}_r\cdot\vec{c}}{\rho}\left(\lambda_r\vec{\xi}^2 - 1\right)\right),
\end{aligned} \tag{2}$$

and

$$\begin{aligned}
\tilde{M}_{eq} &= M_{eq} + M_{eq}^+, \\
M_{eq} &= \rho\left(\frac{\lambda_{eq}}{\pi}\right)^{\frac{3}{2}} e^{-\lambda_{eq}\vec{c}^2}\frac{\lambda_{eq}}{\pi}e^{-\lambda_{eq}\vec{\xi}^2}, \\
M_{eq}^+ &= M_{eq}\left(\omega_0\frac{4\lambda_{eq}^2\vec{q}_t\cdot\vec{c}}{15\rho}\left(2\lambda_{eq}\vec{c}^2 - 5\right) + \omega_1\frac{4(1-\sigma)\lambda_{eq}^2\vec{q}_r\cdot\vec{c}}{\rho}\left(\lambda_{eq}\vec{\xi}^2 - 1\right)\right),
\end{aligned} \tag{3}$$

where $\lambda_{t,r,eq} = 1/(2RT_{t,r,eq})$, $\tau = \mu(T_t)/(\rho R T_t)$ is the translational collision time with $\mu(T_t)$ as the dynamic viscosity coefficient and the subscript t, r, qe in $T_{t,r,eq}$ represent translational, rotational and equilibrium temperature, respectively. Z_{rot} is the rotational relaxation collision number which is related to the ratio of elastic collision frequency to inelastic collision frequency. The parameter σ depends on the molecular potential, and ω_0 and ω_1 are set to have proper relaxation of heat flux. In this paper, these coefficients adopt the values $\sigma = 1/1.55$, $\omega_0 = 0.2354$, $\omega_1 = 0.3049$ for nitrogen [21].

2.2. Unified gas-kinetic particle method

2.2.1. General framework of the unified gas-kinetic particle method

Re-write the Rykov kinetic model equation in a more convenient form,

$$\frac{\partial f}{\partial t} + \vec{v}\cdot\nabla_{\vec{x}} f = \frac{M^* - f}{\tau}, \tag{4}$$

where M^* is defined as,

$$M^* = \tilde{M}_t + \frac{\tilde{M}_{eq} - \tilde{M}_t}{Z_{rot}} \tag{5}$$

Now the Rykov kinetic model has the BGK-type form with a different equilibrium distribution function. With a local constant collision time τ, the integral solution of Eq. (4) can be written as,

$$f(\vec{x},t,\vec{v},\vec{\xi}) = \frac{1}{\tau}\int_0^t e^{-(t-t')/\tau} M^*(\vec{x}',t',\vec{v},\vec{\xi})dt' + e^{-t/\tau} f_0(\vec{x}-\vec{v}t), \tag{6}$$

where f_0 is the initial distribution function at $t=0$ and M^* is defined as the convex combination of two modified equilibrium distribution function in Eq. (5). The equilibrium distribution is integrated along the characteristics $\vec{x}' = \vec{x} + \vec{v}(t'-t)$.

The UGKP is constructed on a discretized physical space $\sum_i \Omega_i \subset \mathcal{R}^3$ and discretized time $t^n \in \mathcal{R}^+$. The cell averaged macroscopic variables $\vec{W}_i = (\rho_i, \rho_i\vec{U}_i, \rho_i E_i, \rho_i E_{rot,i})$ on a physical cell Ω_i are defined as

$$\vec{W}_i = \frac{1}{|\Omega_i|}\int_{\Omega_i} \vec{W}(\vec{x})d\vec{x}.$$

The cell averaged macroscopic variables $\vec{W}_i$ are evolved by the macroscopic governing equations which can be obtained by taking moments of Eq. (4)

$$\vec{W}_i^{n+1} = \vec{W}_i^n - \frac{\Delta t}{|\Omega_i|}\sum_{l_s\in\partial\Omega_i} |l_s|\vec{F}_s + \vec{S}_i, \tag{7}$$

where $l_s \in \partial\Omega_i$ is the cell interface with centre $\vec{x}_s$ and outer unit normal vector $\vec{n}_s$. The flux function for the macroscopic variables at the cell interfaces are constructed by Eq. (6),

$$\begin{aligned}\vec{F}_s &= \frac{1}{\Delta t}\int_0^{\Delta t}\int f(\vec{x}_s,t,\vec{v},\vec{\xi})\vec{v}\cdot\vec{n}_s\vec{\psi}d\Xi dt \\ &= \frac{1}{\Delta t}\int_0^{\Delta t}\int \left[\frac{1}{\tau}\int_0^t e^{(t'-t)/\tau} M^*(\vec{x}_s',t',\vec{v},\vec{\xi})dt' + e^{-t/\tau} f_0(\vec{x}_s-\vec{v}t)\right]\vec{v}\cdot\vec{n}_s\vec{\psi}d\Xi dt,\end{aligned} \tag{8}$$

with the characteristics $\vec{x}_s' = \vec{x}_s + \vec{v}(t'-t)$. The equilibrium flux terms related to the Maxwellian distribution are denoted as $\vec{F}_{eq,s}$,

$$\vec{F}_{eq,s} \overset{\text{def}}{=} \frac{1}{\Delta t}\int_0^{\Delta t}\int \frac{1}{\tau}\int_0^t e^{(t'-t)/\tau} M^*(\vec{x}_s',t',\vec{v},\vec{\xi})dt'\vec{v}\cdot\vec{n}_s\vec{\psi}d\Xi dt, \tag{9}$$

and the flux terms related to the initial distribution are $\vec{F}_{fr,s}$,

$$\vec{F}_{fr,s} \overset{\text{def}}{=} \frac{1}{\Delta t}\int_0^{\Delta t}\int e^{-t/\tau} f_0(\vec{x}_s-\vec{v}t)\vec{v}\cdot\vec{n}_s\vec{\psi}d\Xi dt. \tag{10}$$

The source term $\vec{S}$ is

$$\vec{S} = \int_0^{\Delta t}\int \frac{M^*-f}{\tau}\vec{\psi}d\Xi dt = \int_{t^n}^{t^{n+1}} \vec{s}dt,$$

where $\vec{s}$ can be expressed as

$$\vec{s} = \left(0,0,0,0,\frac{\rho E_{rot}^{eq} - \rho E_{rot}}{Z_{rot}\tau}\right)^T.$$

The equilibrium rotational energy ρE_{rot}^{eq} is determined under the assumption $T_r = T_t = T_{eq}$ such that

$$\rho E_{rot}^{eq} = \frac{K_r\rho}{4\lambda_{eq}} \quad \text{and} \quad \lambda_{eq} = \frac{K_r+3}{4}\frac{\rho}{\rho E - \frac{1}{2}\rho(U^2+V^2+W^2)}. \tag{11}$$

Here K_r is the rotational degrees of freedom.

In the UGKP method, the equilibrium flux term $\vec{F}_{eq,s}$ can be calculated analytically and the free streaming flux term $\vec{F}_{fr,s}$ is calculated by the simulating particles. Specifically, the updates of macroscopic variables will become,

$$\vec{W}_i^{n+1} = \vec{W}_i^n - \frac{\Delta t}{|\Omega_i|}\sum_{l_s\in\partial\Omega_i}|l_s|\vec{F}_{eq,s} + \frac{\Delta t}{|\Omega_i|}\vec{W}_{fr,i} + \vec{S}_i,$$

where $\vec{W}_{fr,i}$ is the net free streaming flow of cell i calculated by counting the particles passing through the cell interface during a time step. The detailed calculation method for $\vec{F}_{eq,s}$, $\vec{W}_{fr,i}$ and the update with source term $\vec{S}_i$ will be given in section 2.2.2, section 2.2.3 and section 2.2.4, respectively.

The particle dynamics in the UGKP method is constructed based on the Rykov kinetic model equation. The main idea of the UGKP method is to track particle trajectory until the collision happens. Once the particle collides with other particles, it will be merged into the macroscopic flow quantities, and get re-sampled from the updated macroscopic flow variables at the beginning of the next time step.

2.2.2. The construction of equilibrium flux

In this subsection, the construction of the equilibrium flux $\vec{F}_{eq,s}$ will be presented. Recall that

$$\begin{aligned} M^* &= \tilde{M}_t + \frac{\tilde{M}_{eq} - \tilde{M}_t}{Z_{rot}} \\ &= M_t + \frac{M_{eq} - M_t}{Z_{rot}} + M_q, \end{aligned} \tag{12}$$

and

$$M_q = \frac{Z_{rot}-1}{Z_{rot}}M_t^+ + \frac{1}{Z_{rot}}M_{eq}^+$$

as the correction term for the heat flux. A straightforward method to construct the equilibrium flux is to expand the first two terms in Eq. (12) around the cell interface, and this was the construction method used in the diatomic UGKS [21]. Based on the following lemma, the calculation of the equilibrium can be simplified.

Lemma 2.1. *If M_t and M_{eq} are defined as in Eq. (2) and Eq. (3) then we have*

$$\frac{M_{eq}-M_t}{Z_{rot}} = O(\tau) \quad or \quad \frac{M_{eq}-M_t}{Z_{rot}} \ll \tau, \quad \tau \to 0.$$

Proof. Firstly, consider the case that $Z_{rot} = O(\tau^{-1})$ or $Z_{rot} \gg \tau^{-1}$, we can obtain

$$\frac{M_{eq}-M_t}{Z_{rot}} = O(\tau) \quad \text{or} \quad \frac{M_{eq}-M_t}{Z_{rot}} \ll \tau$$

Next, for the other case that $Z_{rot} \ll \tau^{-1}$, we have $Z_{rot}\tau^2 \ll \tau$. The leading order approximation gives [31],

$$T_t - T_r = -\frac{2}{3}Z_{rot}\tau T_{eq}\nabla_{\vec{x}}\cdot\vec{U}, \tag{13}$$

from which $|T_{eq}-T_t|/Z_{rot} = O(\tau)$ can be estimated. The linearized Maxwell distribution function M_t around the equilibrium temperature T_{eq} becomes

$$\begin{aligned} M_t =& M_{eq} + \frac{T_t - T_{eq}}{T_{eq}}M_{eq}\left[\left(\frac{\vec{c}^2}{2RT_{eq}} - \frac{3}{2}\right) - \frac{3}{K_r}\left(\frac{\vec{\xi}^2}{2RT_{eq}} - \frac{K_r}{2}\right)\right] + O(|T_{eq}-T_t|^2) \\ =& M_{eq} + \frac{T_t - T_{eq}}{T_{eq}}M_{eq}\left[\left(\frac{\vec{c}^2}{2RT_{eq}} - \frac{3}{2}\right) - \frac{3}{K_r}\left(\frac{\vec{\xi}^2}{2RT_{eq}} - \frac{K_r}{2}\right)\right] + O(Z_{rot}^2\tau^2). \end{aligned}$$

Hence,

$$\frac{M_{eq}-M_t}{Z_{rot}} = \frac{T_t - T_{eq}}{Z_{rot}}\frac{M_{eq}}{T_{eq}}\left[\left(\frac{\vec{c}^2}{2RT_{eq}} - \frac{3}{2}\right) - \frac{3}{K_r}\left(\frac{\vec{\xi}^2}{2RT_{eq}} - \frac{K_r}{2}\right)\right] + O(Z_{rot}\tau^2) = O(\tau) \quad \square$$

Therefore, the second term $(M_{eq}-M_t)/Z_{rot}$ in Eq. (12) is of order τ. Since M_q is also a high order term, only the first term of M^*, i.e., M_t, is expanded in the calculation of the equilibrium flux. The Maxwellian distribution M_t is expanded around $\vec{x}_0$ as

$$
\begin{aligned}
M_t(\vec{x},t,\vec{v},\vec{\xi}) =& M_t(\vec{x}_s,t^n,\vec{v},\vec{\xi}) + (1-H[\bar{x}])\frac{\partial^l}{\partial x}M_t(\vec{x}_s,t^n,\vec{v},\vec{\xi})\bar{x} + H[\bar{x}]\frac{\partial^r}{\partial x}M_t(\vec{x}_s,t^n,\vec{v},\vec{\xi})\bar{x} \\
&+ \frac{\partial}{\partial y}M_t(\vec{x}_s,t^n,\vec{v},\vec{\xi})\bar{y} + \frac{\partial}{\partial z}M_t(\vec{x}_s,t^n,\vec{v},\vec{\xi})\bar{z} + \frac{\partial}{\partial t}M_t(\vec{x}_s,t^n,\vec{v},\vec{\xi})(t-t^n) \\
=& M_t(\vec{x}_s,t^n,\vec{v},\vec{\xi})\left[1 + (1-H[\bar{x}])a^l\bar{x} + H[\bar{x}]a^r\bar{x} + b\bar{y} + c\bar{z} + A(t-t^n)\right],
\end{aligned} \tag{14}
$$

where $\bar{x} = x - x_s$, $\bar{y} = y - y_s$, and $\bar{z} = z - z_s$. The derivative functions of M_t, denoted as a^l, a^r, b, c, and A have the following form

$$
\begin{aligned}
a^l &= a_1^l + a_2^l u + a_3^l v + a_4^l w + \frac{1}{2}a_5^l\vec{v}^2 + \frac{1}{2}a_6^l\vec{\xi}^2, \\
a^r &= a_1^r + a_2^r u + a_3^r v + a_4^r w + \frac{1}{2}a_5^r\vec{v}^2 + \frac{1}{2}a_6^r\vec{\xi}^2, \\
&\cdots \\
A &= A_1 + A_2 u + A_3 v + A_4 w + \frac{1}{2}A_5\vec{v}^2 + \frac{1}{2}A_6\vec{\xi}^2.
\end{aligned}
$$

The Heaviside function $H[x]$ is defined by

$$
H[x] = \begin{cases} 1 & x > 0, \\ 0 & x \le 0. \end{cases}
$$

The Maxwellian at $\vec{x}_0$ and its derivative functions can be obtained from the reconstructed macroscopic variables. In this paper, the van Leer limiter is used for reconstruction,

$$
s = (\mathrm{sign}(s_l) + \mathrm{sign}(s_r))\frac{|s_l||s_r|}{|s_l| + |s_r|}, \tag{15}
$$

where s, s_l, and s_r are the slopes of macroscopic variables. The Maxwellian distribution M_t at cell interface can be obtained from the macroscopic flow variables, which are evaluated by

$$
\vec{W}_s = \int \vec{\psi}\left(M_t^l H[\bar{u}] + M_t^r(1 - H[\bar{u}])\right) d\Xi, \tag{16}
$$

where $\bar{u} = \vec{u}\cdot\vec{n}_s$.

The derivative functions a^l, a^r, b, c, A are calculated from the spatial and time derivatives of M_t. Taking a as an example,

$$
a = \frac{1}{M_t}\left(\frac{\partial M_t}{\partial x}\right),
$$

and

$$
\begin{aligned}
a_6 &= 4\frac{\lambda_r^2}{K_r}\left(2\frac{\partial \rho E_{rot}}{\partial x} - \frac{1}{2}\frac{K_r}{\lambda_r}\frac{\partial \rho}{\partial x}\right), \\
a_5 &= \frac{4\lambda_t^2}{3}\left(B - 2UR_1 - 2VR_2 - 2WR_3\right), \\
a_4 &= 2\lambda_t R_3 - a_5 W, \\
a_3 &= 2\lambda_t R_2 - a_5 V, \\
a_2 &= 2\lambda_t R_1 - a_5 U, \\
a_1 &= \frac{\partial \rho}{\partial x} - a_2 U - a_3 V - a_4 W - \frac{1}{2}a_5(\vec{U}^2 + \frac{3}{2\lambda_t}) - \frac{1}{2}a_6\frac{K_r}{2\lambda_r},
\end{aligned}
$$

with the defined variables

$$
\begin{aligned}
B &= 2\frac{\partial(\rho E - \rho E_{rot})}{\partial x} - (\vec{U}^2 + \frac{3}{2\lambda_t})\frac{\partial \rho}{\partial x}, \\
R_1 &= \frac{\partial \rho U}{\partial x} - U\frac{\partial \rho}{\partial x}, \\
R_2 &= \frac{\partial \rho V}{\partial x} - V\frac{\partial \rho}{\partial x}, \\
R_3 &= \frac{\partial \rho W}{\partial x} - W\frac{\partial \rho}{\partial x},
\end{aligned}
$$

where the derivatives of macroscopic quantities are evaluated at $(\vec{x}_s, t^n)$. The time derivatives of macroscopic variables are determined by the conservative requirements on the first order Chapman-Enskog expansion [32],

$$\left(\frac{\partial \vec{W}_s}{\partial t}\right) = -\int \left(a^l \bar{u} H[\bar{u}] + a^r \bar{u}(1 - H[\bar{u}]) + b\bar{v} + c\bar{w}\right) M_t \vec{\psi} d\Xi.$$

Once the Maxwellian distribution at cell interface and its derivative functions are determined, the equilibrium flux function Eq. (9) can be obtained using the expansion Eq. (14) for the interface distribution function, which gives

$$\begin{aligned}\vec{F}_{eq,s} = \int \vec{v}\cdot\vec{n}_s\vec{\psi}\Big\{ & C_1 M^*(\vec{x}_s, t^n, \vec{v}, \vec{\xi}) + C_2\left[a^l H[\bar{u}] + a^r(1 - H[\bar{u}])\right]\bar{u} M_t(\vec{x}_s, t^n, \vec{v}, \vec{\xi}) \\ & + C_2(b\bar{v} + c\bar{w}) M_t(\vec{x}_s, t^n, \vec{v}, \vec{\xi}) + C_3 A M_t(\vec{x}_s, t^n, \vec{v}, \vec{\xi})\Big\} d\Xi,\end{aligned} \tag{17}$$

where the time integration related coefficients are

$$\begin{aligned} C_1 &= 1 - \frac{\tau}{\Delta t}\left(1 - e^{-\Delta t/\tau}\right), \\ C_2 &= -\tau + \frac{2\tau^2}{\Delta t} - e^{-\Delta t/\tau}\left(\frac{2\tau^2}{\Delta t} + \tau\right), \\ C_3 &= \frac{1}{2}\Delta t - \tau + \frac{\tau^2}{\Delta t}\left(1 - e^{-\Delta t/\tau}\right). \end{aligned}$$

Theoretically, the modified term M_q in M^* only contributes to the heat conduction coefficient in the energy flux. By following the treatment in [33], the calculation of equilibrium flux can be simplified. We can ignore the modified terms and correct the heat flux by adjusting the derivatives of temperature. Based on the Chapman-Enskog expansion and the linearisation around translation temperature T_t [34], the heat fluxes $\vec{q}_t$ and $\vec{q}_r$ become

$$\begin{aligned} \vec{q}_t &= -\frac{15R}{4}\mu(T_t)(1 + 0.5(1 - \omega_0)Z_{rot}^{-1})^{-1}\nabla_{\vec{x}} T_t, \\ \vec{q}_r &= -R\mu(T_t)(\sigma + (1 - \sigma)(1 - \omega_1)Z_{rot}^{-1})^{-1}\nabla_{\vec{x}} T_r, \end{aligned} \tag{18}$$

where $\mu(T_t) = \tau p_t$ and the pressure p_t is related to the translational temperature only through $p_t = \rho R T_t$. We can modify the computed coefficients in the expansion of Maxwellian to get the above heat fluxes by re-scaling the translational and rotational temperature gradients, such as changing $a_5 = 2\partial_x \lambda_t$ and $a_6 = 2\partial_x \lambda_r$ to

$$\begin{aligned} \tilde{a}_6 &= \frac{3}{2}(\sigma + (1 - \sigma)(1 - \omega_1)Z_{rot}^{-1})^{-1} a_6 \\ \tilde{a}_5 &= (1 + 0.5(1 - \omega_0)Z_{rot}^{-1})^{-1} a_5. \end{aligned}$$

Thus, only few additional floating point operations are needed for each spatial slope reconstruction to correct the heat flux, and the final form of $\vec{F}_{eq,s}$ becomes

$$\begin{aligned}\vec{F}_{eq,s} = \int \vec{v}\cdot\vec{n}_s\vec{\psi}\Big\{ & C_1\left(M_t(\vec{x}_s, t^n, \vec{v}, \vec{\xi}) + \frac{M_{eq}(\vec{x}_s, t^n, \vec{v}, \vec{\xi}) - M_t(\vec{x}_s, t^n, \vec{v}, \vec{\xi})}{Z_{rot}}\right) \\ & + C_2\left[a^l H[\bar{u}] + a^r(1 - H[\bar{u}])\right]\bar{u} M_t(\vec{x}_s, t^n, \vec{v}, \vec{\xi}) \\ & + C_2(b\bar{v} + c\bar{w}) M_t(\vec{x}_s, t^n, \vec{v}, \vec{\xi}) + C_3 A M_t(\vec{x}_s, t^n, \vec{v}, \vec{\xi})\Big\} d\Xi,\end{aligned} \tag{19}$$

with the above scaled coefficients.

2.2.3. The evolution of particles

The simulation particle $P_k(m_k, \vec{x}_k, \vec{v}_k, e_k, t_{f,k}, \omega_k, \kappa_k)$ is represented by its mass m_k, position coordinate $\vec{x}_k$, velocity coordinate $\vec{v}_k$, free streaming time $t_{f,k}$ and internal energy e_k. ω_k and κ_k are the weights coming from the Rykov kinetic model. Recall that the evolution of particles follows the integral form of the Rykov model,

$$f(\vec{x}, t, \vec{v}, \vec{\xi}) = \frac{1}{\tau}\int_0^t e^{-(t-t')/\tau} M^*(\vec{x}', t', \vec{v}, \vec{\xi}) dt' + e^{-t/\tau} f_0(\vec{x} - \vec{v}t). \tag{20}$$

The Maxwellian distribution function M^* around the interface can be expanded as

$$M^*(\vec{x}', t', \vec{v}, \vec{\xi}) = M^*(\vec{x}, t, \vec{v}, \vec{\xi}) + \nabla_{\vec{x}} M^*(\vec{x}, t, \vec{v}, \vec{\xi}) \cdot (\vec{x}' - \vec{x}) + \partial_t M^*(\vec{x}, t, \vec{v}, \vec{\xi}) t' + O((\vec{x}' - \vec{x})^2, t'^2).$$

The integral solution becomes

$$f(\vec{x}, t, \vec{v}, \vec{\xi}) = (1 - e^{-t/\tau}) M^+(\vec{x}, t, \vec{v}, \vec{\xi}) + e^{-t/\tau} f_0(\vec{x} - \vec{v}t). \tag{21}$$

A first order approximation of M^+ can be expressed as

$$M^+(\vec{x}, t, \vec{v}, \vec{\xi}) = M^*(\vec{x}, t, \vec{v}, \vec{\xi}), \tag{22}$$

and the second order expansion gives

$$M^+(\vec{x}, t, \vec{v}, \vec{\xi}) = M^*(\vec{x}, t, \vec{v}, \vec{\xi}) + \frac{e^{-t/\tau}(t + \tau) - \tau}{1 - e^{-t/\tau}} (\partial_t M^*(\vec{x}, t, \vec{v}, \vec{\xi}) + \vec{v} \cdot \nabla_{\vec{x}} M^*(\vec{x}, t, \vec{v}, \vec{\xi})). \tag{23}$$

Above M^+ is named as the hydrodynamic distribution function with analytical formulation. For both UGKP and UGKWP method, the approximation (22) for M^+ is used for a simple particle-sampling algorithm [35]. The particle evolution equation in Eq. (21) means that the simulation particle has a probability of $e^{-t/\tau}$ to free stream, and has a probability of $(1 - e^{-t/\tau})$ to collide with other particle, and the post-collided particle velocity follows the distribution $M^+(\vec{x}, t, \vec{v}, \vec{\xi})$. The stop time for the free streaming to follow the distribution M^+ is called the first collision time t_c. The cumulative distribution function of the first collision time is

$$F(t_c < t) = 1 - \exp(-t/\tau), \tag{24}$$

from which t_c can be sampled as $t_c = -\tau \ln(\eta)$ with η generated from a uniform distribution $U(0, 1)$. For a particle P_k, the free streaming time can be given as,

$$t_{f,k} = \begin{cases} -\tau \ln(\eta) & \text{if } -\tau \ln(\eta) < \Delta t, \\ \Delta t & \text{if } -\tau \ln(\eta) > \Delta t, \end{cases} \tag{25}$$

where Δt is the time step. Note that $t_{f,k}$ is just the free streaming time of the particle within the current time step, but not the total free stream time of the particle. In a numerical time step from t^n to t^{n+1}, all simulating particles in UGKP method can be categorized into two groups: the **collisionless particle** P^f and the **collisional particle** P^c. The categorization is based on the relative values between the free streaming time t_f and the time step Δt. More specifically, the collisionless particle is defined as the particle whose free streaming time t_f being greater than or equal to the time step Δt, and the collisional particle is defined as the particle whose free streaming time t_f being smaller than Δt. For the collisionless particle, its trajectory is fully tracked during the whole time step. For collisional particle, the particle trajectory is tracked till t_f. Then the particle's mass, momentum, and energy are merged into the macroscopic quantities in that cell and the simulation particle gets eliminated. Those eliminated particles will get re-sampled once the updated macroscopic quantities $\vec{W}^{n+1}$ are obtained. As shown in Eq. (21), the re-sampled particles follow the hydrodynamic distribution M^+ and therefore they are defined as **hydro-particle** P^h. The macroscopic quantities corresponding to the hydro-particles are defined as **hydro-quantities** $\vec{W}^h$. The hydro-particles will be sampled at the beginning of each time step and become the candidates for collisionless/collisional particles again in the next time step evolution according to their newly-sampled t_f.

At the beginning of each step, we need to sample particles from M^* defined in Eq. (5). For cell Ω_i with hydro quantities $\vec{W}_i^h = \left(\rho_i^h, \rho_i^h U_i^h, \rho_i^h V_i^h, \rho_i^h W_i^h, \rho_i^h E_i^h, \rho_i^h E_{rot,i}^h\right)^T$, using the stratification for variance reduction, hydro-particles can be sampled from the modified Maxwellian distribution $\tilde{M}_t$ with a total mass of $((Z_{rot} - 1)/(Z_{rot}))\rho_i^h|\Omega_i|$ and the modified Maxwellian distribution $\tilde{M}_{eq}$ with a total mass of $\rho_i^h|\Omega_i|/Z_{rot}$, respectively.

Taking $\tilde{M}_t$ as an example, the reduced distribution function for rotational variable $\vec{\xi}$ can be written as

$$G_t = \int \tilde{M}_t d\vec{\xi} = G_m(\lambda_t) \left[1 + \frac{4\lambda_t^2 \vec{q}_t \cdot \vec{c}}{15\rho} \left(2\lambda_t \vec{c}^2 - 5\right)\right],$$

$$R_t = \int \vec{\xi}^2 \tilde{M}_t d\vec{\xi} = \frac{K_r}{2\lambda_r} G_m(\lambda_t) \left[1 + \frac{4\lambda_t^2 \vec{q}_t \cdot \vec{c}}{15\rho} \left(2\lambda_t \vec{c}^2 - 5\right) + \frac{8(1 - \sigma)\lambda_t \lambda_r \vec{q}_r \cdot \vec{c}}{K_r \rho}\right]$$

with

$$G_m(\lambda) = \rho \left(\frac{\lambda}{\pi}\right)^{\frac{3}{2}} e^{-\lambda \vec{c}^2}.$$

Following the idea of importance sampling, the hydro quantities $\vec{W}_i^h$ from the moments of the above specified distributions can be rewritten as,

$$\begin{aligned}\vec{W}_i^h &= \int \begin{pmatrix} G_t \\ \vec{v}G_t \\ \frac{\vec{v}^2}{2}G_t + \frac{1}{2}R_t \\ \frac{1}{2}R_t \end{pmatrix}_i d\vec{v} = \int \begin{pmatrix} \frac{G_t}{G_m}G_m \\ \vec{v}\frac{G_t}{G_m}G_m \\ \left(\frac{\vec{v}^2}{2}\frac{G_t}{G_m} + \frac{1}{2}\frac{R_t}{G_m}\right)G_m \\ \frac{1}{2}\frac{R_t}{G_m}G_m \end{pmatrix}_i d\vec{v} \\ &\approx \sum \begin{pmatrix} \omega_k \frac{m_p}{|\Omega|_j} \\ \omega_k \frac{m_p \vec{v}_k}{|\Omega|_i} \\ \omega_k \frac{m_p \vec{v}_k^2}{2|\Omega|_i} + \kappa_k \frac{m_p e_k}{2|\Omega|_i} \\ \kappa_k \frac{m_p e_k}{2|\Omega|_i} \end{pmatrix}.\end{aligned} \tag{26}$$

In order to recover the gas distribution function on the microscopic level, the sampled particles P_k, $k = 1, ..., N_i$, follow

$$\begin{aligned} m_p &= \frac{Z_{rot}-1}{Z_{rot}}\frac{\rho_i^h|\Omega|_i}{N_i}, \quad \vec{x}_k \sim \mathrm{U}(\Omega_i), \quad e_k = \frac{K_r}{2\lambda_{r,i}}, \\ \vec{v}_k &= \vec{U}_i + (-\ln(\vec{\eta}_1)/\lambda_{t,i})^{1/2}\cos(2\pi\vec{\eta}_2), \quad \vec{\eta}_{1,2} \sim \mathrm{U}(0,1)^3, \end{aligned} \tag{27}$$

where $\mathrm{U}(\Omega_i)$ is the uniform distribution on Ω_i and $\mathrm{U}(0,1)^3$ is the uniform distribution on $(0,1)^3$. The symmetric sampling is adopted here to reduce the variance. To be more specific, with the same $\vec{\eta}_{1,2}$, a symmetric particle will be sampled simultaneously. The microscopic velocity of the symmetric particle is

$$\vec{v}_k' = \vec{U}_i - (-\ln(\vec{\eta}_1)/\lambda_{t,i})^{1/2}\cos(2\pi\vec{\eta}_2). \tag{28}$$

The addition weights ω_k and κ_k are required in order to make the macroscopic quantities of the sampled particles P_k consistent with the macro quantities $\vec{W}_i^h$. As shown in Eq. (26), ω_k and κ_k are determined by the coefficients G_t/G_m and R_t/G_m, respectively, i.e.

$$\begin{aligned} \omega_k &= 1 + \frac{4\lambda_t^2 \vec{q}_t \cdot \vec{c}_k}{15\rho}\left(2\lambda_t \vec{c}_k^2 - 5\right), \\ \kappa_k &= 1 + \frac{4\lambda_t^2 \vec{q}_t \cdot \vec{c}_k}{15\rho}\left(2\lambda_t \vec{c}_k^2 - 5\right) + \frac{8(1-\sigma)\lambda_t\lambda_r \vec{q}_r \cdot \vec{c}_k}{K_r\rho}. \end{aligned} \tag{29}$$

Similarly, the particles from $\rho_i^h|\Omega_i|/Z_{rot}$ can be sampled as well with $e_k = \frac{K_r}{2\lambda_{eq,i}}$.

Now all the quantities of P_k are determined. The particle will take free streaming for a period of t_{fk},

$$\vec{x}_k^{n+1} = \vec{x}_k^n + \vec{v}_k t_{f,k}. \tag{30}$$

The net free streaming flow of cell i at the next step can be calculated by counting the particles passing through the cell interface, which can be written as,

$$\vec{W}_{fr,i} = \frac{1}{\Delta t}\left(\sum_{k\in P_{\partial\Omega_i^+}} \vec{W}_{P_k} - \sum_{k\in P_{\partial\Omega_i^-}} \vec{W}_{P_k}\right), \tag{31}$$

where $\vec{W}_{P_k} = \left(\omega_k m_k, \omega_k m_k \vec{v}_k, \frac{1}{2}m_k\left(\omega_k \vec{v}_k^2 + \kappa_k e_k\right), \frac{1}{2}m_k\kappa_k e_k\right)^T$, $P_{\partial\Omega_i^+}$ is the index set of the particles streaming into cell Ω_i during a time step, and $P_{\partial\Omega_i^-}$ is the index set of the particles streaming out of cell Ω_i.

2.2.4. The update of macroscopic flow variables with source term

Since the source term in the rotational energy, ρE_{rot} can be updated using a semi-implicit scheme. Based on $\vec{W}^*$ as defined by

$$\vec{W}_i^* = \vec{W}_i^n + \frac{\Delta t}{|\Omega_i|}\left(\sum_{l_s\in\partial\Omega_i} |l_s|\vec{F}_{eq,s} + \vec{W}_{fr,i}\right), \tag{32}$$

$\rho^{n+1}, (\rho\vec{U})^{n+1}$ and $(\rho E)^{n+1}$ can be updated. Then, from Eq. (11), the equilibrium rotational energy $(\rho E_{rot}^{eq})^{n+1}$ can be obtained as well, from which the source term for rotational energy can be approximated as,

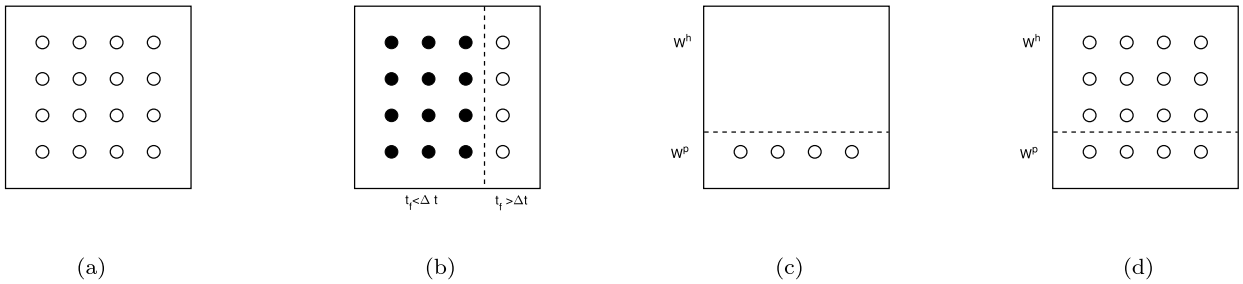

Fig. 1. Diagram to illustrate the composition of the particles during time evolution in the UGKP method. (a) Initial field; (b) classification of the collisionless particles (white circle) and collisional particles (solid circle) according to the free transport time t_f; (c) update solution at macroscopic level; (d) update solution at microscopic level.

$$S = \frac{\Delta t}{2}\left(\frac{2(\rho E_{rot}^{eq})^{n+1} - (\rho E_{rot})^{*} - (\rho E_{rot})^{n+1}}{(Z_{rot}\tau)^{*}}\right), \tag{33}$$

thus

$$(\rho E_{rot})^{n+1} = \left(1 + \frac{\Delta t}{2(Z_{rot}\tau)^{*}}\right)^{-1}\left((\rho E_{rot})^{*} + \frac{\Delta t}{2}\left(\frac{2(\rho E_{rot}^{eq})^{n+1} - (\rho E_{rot})^{*}}{(Z_{rot}\tau)^{*}}\right)\right). \tag{34}$$

In UGKP, the evolution of microscopic particle is coupled with the evolution of macroscopic flow variables. The composition of the particles during time evolution in the UGKP method is illustrated in Fig. 1 [27]. The algorithm of UGKP method for diatomic gas can be summarized as follows:

1. Sample the particle quantities $(m_k, \vec{x}_k, \vec{v}_k, e_k, \omega_k, \kappa_k)$ by Eq. (27) and Eq. (29) for each newly added particle P_k from the hydro-quantities $\vec{W}^h$. For the first step, $\vec{W}^h = \vec{W}^{n=0}$ as shown in Fig. 1a.
2. Sample free streaming time $t_{f,k}$ by Eq. (25) for each particle P_k and they will be classified into collisionless particles (white circles in Fig. 1b) and collisional particles (solid circles in Fig. 1b). Then, stream the particles by Eq. (30).
3. Calculate the net free streaming flow $\vec{W}_{fr}$ by Eq. (31), and evaluate the equilibrium flux $\vec{F}^{eq}$ by Eq. (19).
4. Update total macroscopic flow variables $\vec{W}$ by Eq. (32) and Eq. (34). Calculate the macro-quantities of collisionless particles $\vec{W}^p$ by collecting the macro-quantities of collisionless particles, from which the hydro-quantities $\vec{W}^h$ are obtained by $\vec{W}^h = \vec{W} - \vec{W}^p$. [Shown in Fig. 1c]
5. Keep collisionless particles and remove collisional particles, and then go to step 1. Fig. 1d is the initial state in Fig. 1a for the next time step.

2.3. Unified gas-kinetic wave-particle method

The UGKWP method improves UGKP method mainly in the following two aspects:

- The free transport terms in numerical flux contributed by the newly generated collisional hydro-particles can be evaluated analytically;
- Only collisionless hydro-particles are sampled.

Firstly, since the distribution of the hydro-quantities $\vec{W}^h$ is known as M^+, the flux contributed by the free transport of collisional hydro-particles can be evaluated analytically,

$$\sum_s |l_s|\vec{F}_{fr,s} = \sum_s |l_s|\vec{F}^h_{fr,s} + \vec{W}^p_{fr,i},$$

where $\vec{F}^h_{fr,s}$ is the free transport flux contributed by the hydro-quantities [26],

$$\vec{F}^h_{fr,s} = \int\left[C_4 M^+(\vec{x}_s, t^n, \vec{v}, \vec{\xi}) + C_5\vec{v}\cdot\nabla_{\vec{x}}M_t(\vec{x}_s, t^n, \vec{v}, \vec{\xi})\right]\vec{v}\cdot\vec{n}_s\vec{\psi}d\Xi, \tag{35}$$

where M^+ is given in Eq. (23), $C_4 = \frac{\tau}{\Delta t}\left(1 - e^{-\Delta t/\tau}\right) - e^{-\Delta t/\tau}$, and $C_5 = \tau e^{-\Delta t/\tau} - \frac{\tau^2}{\Delta t}(1 - e^{-\Delta t/\tau}) + \frac{1}{2}\Delta t e^{-\Delta t/\tau}$.

Secondly, since the numerical flux contributed by the streaming of collisional particles can be evaluated by $\vec{F}^h_{fr,s}$ analytically, only the collisionless hydro-particle will be sampled. Based on the cumulative distribution function of the first collision time Eq. (24), the collisionless hydro-particles are sampled from $M^+(\vec{W}_i^{n+1})$ with a total mass of $e^{-\Delta t/\tau_i}|\Omega_i|\rho_i^h$.

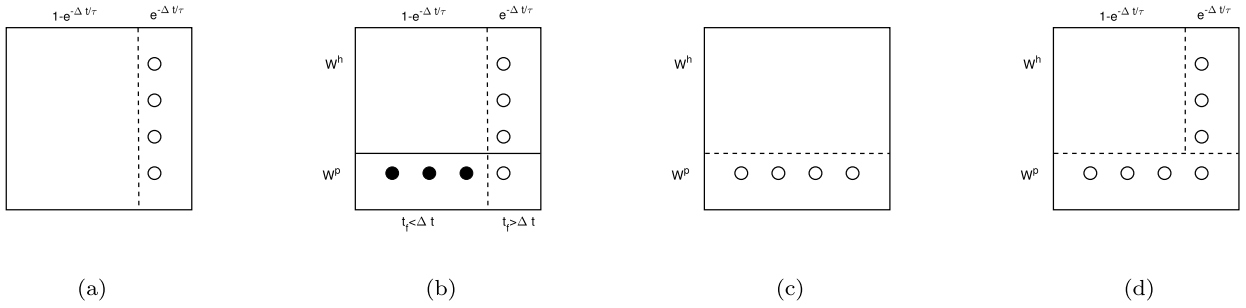

Fig. 2. Diagram to illustrate the composition of the particles during time evolution in the UGKWP method. (a) Initial field; (b) classification of the collisionless and collisional particles for $\vec{W}^p$; (c) update on macroscopic level; (d) update on the microscopic level.

Then, the net free streaming flux contributed by the streaming of all left particles from previous time step and newly generated collisionless particles can be calculated by Eq. (31),

$$\vec{W}^p_{fr,i} = \frac{1}{\Delta t}\left(\sum_{k\in P_{\partial\Omega_i^+}} \vec{W}_{P_k} - \sum_{k\in P_{\partial\Omega_i^-}} \vec{W}_{P_k}\right).$$

Therefore, the evolution of macroscopic flow variables in Eq. (32) now becomes

$$\vec{W}_i^* = \vec{W}_i^n + \frac{\Delta t}{|\Omega_i|}\left(\sum_{l_s\in\partial\Omega_i} |l_s|\vec{F}_{eq,s} + \sum_{l_s\in\partial\Omega_i} |l_s|\vec{F}^h_{fr,s} + \vec{W}^p_{fr,i}\right), \tag{36}$$

from which $\rho^{n+1}, (\rho\vec{U})^{n+1}$ and $(\rho E)^{n+1}$ can be obtained. Following the same calculations in Eq. (33) and Eq. (34), $(\rho E_{rot})^{n+1}$ can be obtained as well. The composition of the particles during time evolution in the UGKWP method is illustrated in Fig. 2 [26]. The algorithm of UGKWP method for diatomic gases can be summarized as follows:

1. Sample the particle quantities $(m_k, \vec{x}_k, \vec{v}_k, e_k, \omega_k, \kappa_k)$ by Eq. (27) and Eq. (29) for each newly added collisionless hydro-particle P_k from the hydro-quantities $e^{-\Delta t/\tau}\vec{W}^h$. These particles are all defined as collisionless particles which have $t_f = \Delta t$. For the first step, $W^h = W^{n=0}$ as shown in Fig. 2a.
2. Sample free streaming time $t_{f,k}$ by Eq. (25) for particles P_k from W^p. These particles are classified into collisionless particles (white circles in Fig. 2b) and collisional particles (solid circles in Fig. 2b). Then, stream all the particles by Eq. (30). For the first step, $W^p = 0$.
3. Calculate the net free streaming flow $\vec{W}_{fr}$ by Eq. (31), and evaluate the equilibrium flux $\vec{F}^{eq}$ and free transport flux $\vec{F}^h_{fr,s}$ by Eq. (19) and Eq. (35), respectively.
4. Update total flow variables $\vec{W}$ by Eq. (36) and Eq. (34). Calculate the macro-quantities of collisionless particles $\vec{W}^p$ by collecting the macro-quantities of collisionless particles, from which the hydro-quantities $\vec{W}^h$ are obtained by $\vec{W}^h = \vec{W} - \vec{W}^p$. [Shown in Fig. 2c]
5. Keep collisionless particles and remove collisional particles. Fig. 2d is the initial state of next time step. Then, the following numerical procedures are the stepes from Fig. 2d -> Fig. 2b -> Fig. 2c -> Fig. 2d.

3. Analysis and discussion

3.1. Collisionless limit

Consider the collisionless limit when $\tau \to \infty$, we have

$$\lim_{\tau\to\infty} C_i = 0, \quad i \in \{1, 2, 3, 4, 5\} \tag{37}$$

Therefore, the equilibrium flux $\vec{F}_{eq}$ and the analytical flux $\vec{F}^h_{fr}$ will be 0. The only contribution to the flux is the net free streaming flux $\vec{W}^p_{fr}$. The free streaming time for the particles becomes

$$\lim_{\tau\to\infty} t_c = \Delta t \tag{38}$$

which means that all the particles will be streaming without collision. And then the UGKWP method degenerates to a collisionless Boltzmann solver.

3.2. Asymptotic behaviour in the continuum regime

In this section, we are going to analyze the asymptotic behaviour of the UGKWP method with diatomic relaxation in continuum regime. For simplicity, the following analysis is based on two-dimensional case. Following the Chapman-Enskog procedure, one can show that the macro description of the Rykov model can be written as [34],

$$\begin{aligned}
&\frac{\partial \rho}{\partial t}+\frac{\partial(\rho U)}{\partial x}+\frac{\partial(\rho V)}{\partial y}=0,\\
&\frac{\partial(\rho U)}{\partial t}+\frac{\partial(\rho U^2+p_t)}{\partial x}+\frac{\partial(\rho UV)}{\partial y}=\frac{\partial \tau_{xx}}{\partial x}+\frac{\partial \tau_{yx}}{\partial y},\\
&\frac{\partial(\rho V)}{\partial t}+\frac{\partial \rho UV}{\partial x}+\frac{\partial(\rho V^2+p_t)}{\partial y}=\frac{\partial \tau_{xy}}{\partial x}+\frac{\partial \tau_{yy}}{\partial y},\\
&\frac{\partial(\rho E)}{\partial t}+\frac{\partial(\rho EU+p_tU)}{\partial x}+\frac{\partial(\rho EV+p_tV)}{\partial y}=\frac{\partial(U\tau_{xx}+V\tau_{xy}+q_x)}{\partial x}+\frac{\partial(U\tau_{yx}+V\tau_{xx}+q_y)}{\partial y},\\
&\frac{\partial(\rho E_r)}{\partial t}+\frac{\partial(\rho E_rU)}{\partial x}+\frac{\partial(\rho E_rV)}{\partial y}=\frac{\partial q_{rx}}{\partial x}+\frac{\partial q_{ry}}{\partial y}+\frac{\rho E_r^{eq}-\rho E_r}{Z_{rot}\tau}.
\end{aligned} \tag{39}$$

Here the viscous and heat conduction terms are

$$\begin{aligned}
&\tau_{xx}=\tau p_t\left[2\frac{\partial U}{\partial x}-\frac{2}{3}\left(\frac{\partial U}{\partial x}+\frac{\partial V}{\partial y}\right)\right],\\
&\tau_{yy}=\tau p_t\left[2\frac{\partial V}{\partial y}-\frac{2}{3}\left(\frac{\partial U}{\partial x}+\frac{\partial V}{\partial y}\right)\right],\\
&\tau_{xy}=\tau_{yx}=\tau p_t\left(\frac{\partial U}{\partial y}+\frac{\partial V}{\partial x}\right)\\
&(q_x,q_y)^T=\vec{q}_r+\vec{q}_t,\\
&(q_{rx},q_{ry})^T=\vec{q}_r,
\end{aligned} \tag{40}$$

where $\vec{q}_r$ and $\vec{q}_t$ are defined in Eq. (18). The pressure $p_t=\rho RT_t$ is only related to the translational temperature.

Proposition 3.1 *(Asymptotic preserving property). Consider a well resolved flow region with $M_t^l=M_t^r$ and $\nabla_{\vec{x}}^l M_t=\nabla_{\vec{x}}^r M_t$, for fixed time Δt, and small τ, the scheme is asymptotically equivalent to, up to $O(\tau^2)$, a first order scheme for the system (39) and (40).*

Proof. The number of particles in UGKWP is proportional to $O(e^{-\Delta t/\tau_i})$. In the hydrodynamic regime $\Delta t >> \tau$, the particles will disappear automatically.

In the free transport flux of hydro-quantities $\vec{F}_{fr,s}^h$ given by Eq. (35), the hydrodynamic distribution function $M^+(\vec{x}_0,t,\vec{v},\vec{\xi})$ becomes

$$M^+(x_0,y_0,t,u,v,\vec{\xi})=M^*-\tau\left(\partial_t M_t+u\partial_x M_t+v\partial_y M_t\right)+O(\tau^2). \tag{41}$$

Substituting Eq. (41) into Eq. (35), the total flux $\vec{F}_{an,s}$ of the macroscopic variables becomes

$$\begin{aligned}
\vec{F}_{an,s}=&\vec{F}_{eq,s}+\vec{F}_{fr,s}^h\\
=&\int u\Big\{(C_1+C_4)M^*+(C_2-\tau C_4+C_5)(u\partial_x M_t+v\partial_y M_t)\\
&+(C_3-\tau C_4)\partial_t M_t\Big\}\vec{\psi}dudvd\vec{\xi}+O(\tau^2)\\
=&\int u\left\{M^*-\tau(u\partial_x M_t+v\partial_y M_t+\partial_t M_t)+\frac{1}{2}\Delta t\partial_t M_t\right\}\vec{\psi}dudvd\vec{\xi}+O(\tau^2).
\end{aligned} \tag{42}$$

If $O(\tau^2)$ terms are neglected, Eq. (42) becomes

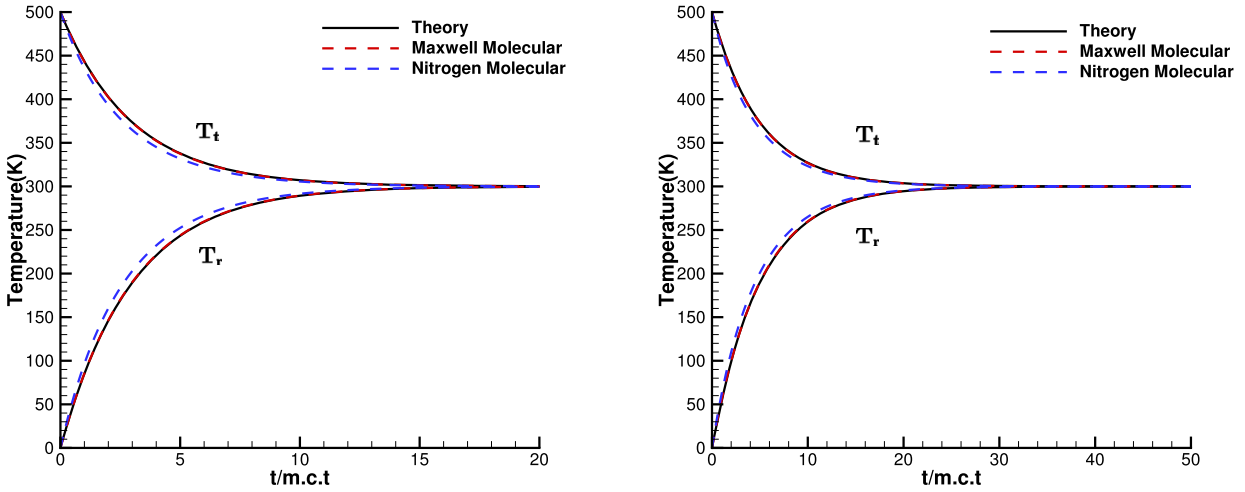

Fig. 3. Rotational relaxation in a homogeneous gas. Left: $Z_{rot} = 3$. Right: $Z_{rot} = 5$.

$$\begin{aligned}\vec{F}_{an,s} &= \int u\left\{M^* - \tau\left(u\partial_x M_t + v\partial_y M_t + \partial_t M_t\right) + \frac{1}{2}\Delta t\partial_t M_t\right\}\vec{\psi}\,du\,dv\,d\vec{\xi} \\ &= \begin{pmatrix} \rho U \\ \rho U^2 + p_t + \tau_{xx} \\ \rho UV + \tau_{xy} \\ \rho E + p_t U + U\tau_{xx} + V\tau_{xy} + q_x \\ \rho E_r + \rho E_r U + q_{rx} \end{pmatrix} + \frac{1}{2}\Delta t \begin{pmatrix} \frac{\partial \rho U}{\partial t} \\ \frac{\partial \rho U^2}{\partial t} + \frac{\partial p_t}{\partial t} \\ \frac{\partial \rho UV}{\partial t} \\ \frac{\partial \rho E}{\partial t} + \frac{\partial p_t U}{\partial t} \\ \frac{\partial \rho E_r}{\partial t} + \frac{\partial \rho E_r U}{\partial t} \end{pmatrix}\end{aligned} \tag{43}$$

It can be observed that the numerical flux is consistent with the flux in system (39) and (40). Therefore, in the continuum regime, the UGKWP method converges to Eq. (39), which is a first order scheme for the system (39) and (40) due to the $1st$-order discretization of the viscous and heat conduction terms. □

For the limiting Euler system with the absence of viscous and heat conduction terms, we can have the following proposition.

Proposition 3.2. *Consider a well resolved flow region with $M_t^l = M_t^r$ and $\nabla_{\vec{x}}^l M_t = \nabla_{\vec{x}}^r M_t$, for fixed time Δt, in the limit $\tau \to 0$, the scheme becomes a second order scheme for the limiting Euler system with the absence of viscous and heat conduction terms in system* (39) *and* (40)*.*

Proof. As $\tau \to 0$, following directly from Eq. (43), we have

$$\vec{F}_{an,s} = \begin{pmatrix} \rho U \\ \rho U^2 + p_t \\ \rho UV \\ \rho E + p_t U \\ \rho E_r + \rho E_r U \end{pmatrix} + \frac{1}{2}\Delta t \begin{pmatrix} \frac{\partial \rho U}{\partial t} \\ \frac{\partial \rho U^2}{\partial t} + \frac{\partial p_t}{\partial t} \\ \frac{\partial \rho UV}{\partial t} \\ \frac{\partial \rho E}{\partial t} + \frac{\partial p_t U}{\partial t} \\ \frac{\partial \rho E_r}{\partial t} + \frac{\partial \rho E_r U}{\partial t} \end{pmatrix}.$$

Combine with the semi-implicit update of source term, it can be observed that this is exactly a second order scheme for the limiting Euler system. □

In the limit of total equilibrium state with $Z_{rot} = 1$, both the translational temperature and the rotational temperature converges to the equilibrium temperature as $\tau \to 0$. From Eq. (13), the pressure p_t can be rewritten as,

$$p_t = p + p_t - p = p - \frac{4}{15} Z_{rot}\tau p\left(\frac{\partial U}{\partial x} + \frac{\partial V}{\partial y}\right). \tag{44}$$

When $Z_{rot} = 1$, the second term on the right hand side of Eq. (44) is exactly the bulk viscosity for rotational degrees of freedom in NS equations.

In the continuum regime with $\Delta t \gg \tau$, for a fixed particle mass m_p, the number of sampled collisionless hydro-particles in cell i is $e^{-\Delta t/\tau_i}|\Omega_i|\rho_i^h/m_p$. And the total simulation particle number N_p in such regime decreases exponentially, $N_p \sim$

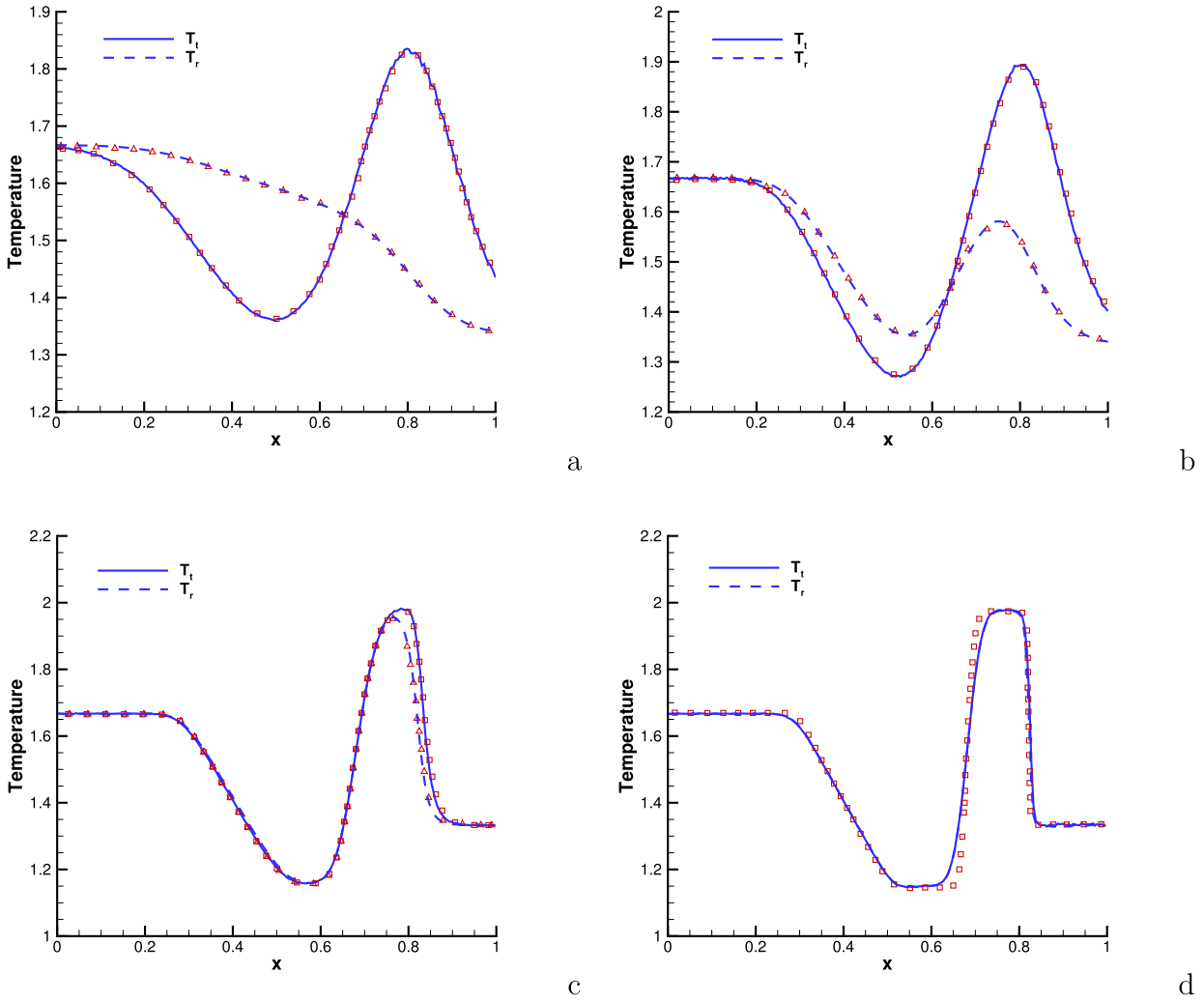

Fig. 4. The temperature profiles at different Kn. (a) Kn = 1.0; (b) Kn = 0.1; (c) Kn = 0.01; (d) Kn = 0.001. The reference solutions are shown in symbol, and the UGKWP solutions are shown in line.

$O(e^{-\Delta t/\tau})$. Therefore, the computational cost of UGKWP in continuum regime becomes comparable to hydrodynamic NS solver, such as recovering GKS for the NS solution [28].

4. Numerical tests

4.1. Rotational relaxation in a homogeneous gas

For a diatomic homogeneous gas with different initial translational T_t and rotational T_r temperature, the system will finally evolve to an equilibrium state with $T_{eq} = T_t = T_r$. The relaxation rate is related to the rotational collision frequency. Since there is no free transport phenomenon in homogeneous case, the governing equation becomes,

$$\frac{\partial f}{\partial t} = \frac{\tilde{M}_t - f}{\tau} + \frac{\tilde{M}_{eq} - \tilde{M}_t}{Z_{rot}\tau}. \tag{45}$$

Multiplying Eq. (45) with ξ^2 and integrating over the velocity and rotational energy space, the time evolution equation of rotational energy becomes

$$\frac{\partial T_r}{\partial t} = \frac{T_{eq} - T_r}{Z_{rot}\tau},$$

from which the analytical solution can be obtained,

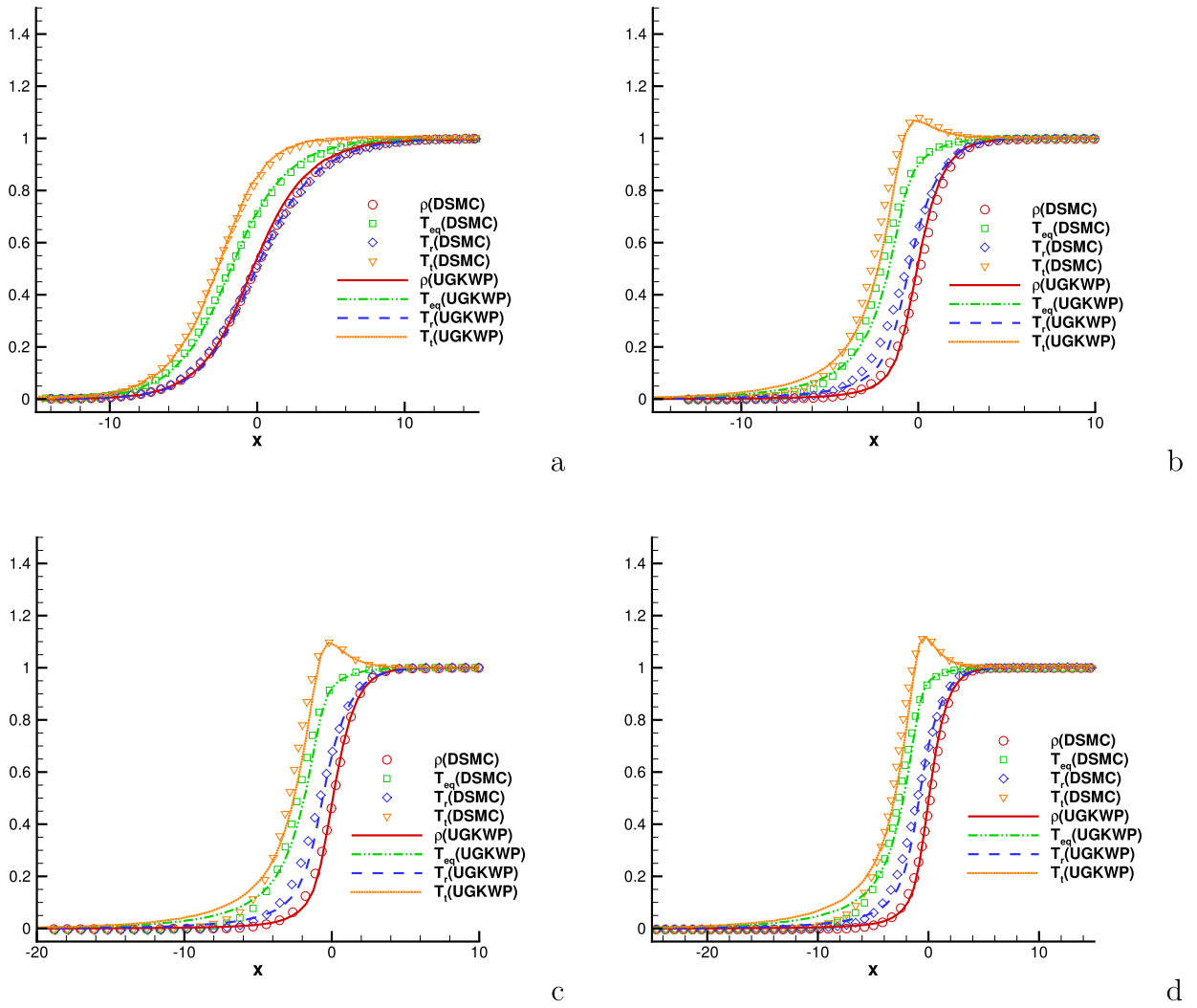

Fig. 5. Comparison of UGKWP and DSMC results of nitrogen shock wave at different Mach number in nitrogen. (a) M = 1.53; (b) M = 4.0; (c) M = 5.0; (d) M = 7.0.

$$T_r(t) = T_{eq} - \left(T_{eq} - T_r(0)\right) e^{-\frac{t}{Z_{rot}\tau}}. \tag{46}$$

In the computation, the variable hard sphere (VHS) model with $\omega = 1$ (Maxwell molecule) and $\omega = 0.72$ (Nitrogen molecule) are used and the relaxation time is approximated as $\tau = \mu/p_t$. Fig. 3 shows the UGKWP solutions at $Z_{rot} = 3$ and 5 for Maxwell molecule and Nitrogen molecule along with the analytical solutions. Note that the analytical solution applies only to Maxwell molecule. The computational results show that the UGKWP solutions for Maxwell molecule match well with the analytical solutions. For the Nitrogen molecule with a greater collision rate, the temperature relaxes to equilibrium a little bit faster. The mean collision time (m.c.t) here is calculated by the equilibrium temperature T_{eq}, which is used to normalize t.

4.2. 1D shock tube problem

To demonstrate the asymptotic preserving property of the UGKWP method, the 1D shock tube problem with various Knudsen numbers will be tested. The computational domain is $[0, 1]$ and initial condition is

$$(\rho, u, T_t, T_r) = \begin{cases} (10.0, 0, 1.667, 1.667) & x \le 0.5, \\ (1.0, 0, 1.333, 1.333) & x > 0.5. \end{cases}$$

The viscous coefficient μ and the rotational collision number Z_{rot} are given as [36],

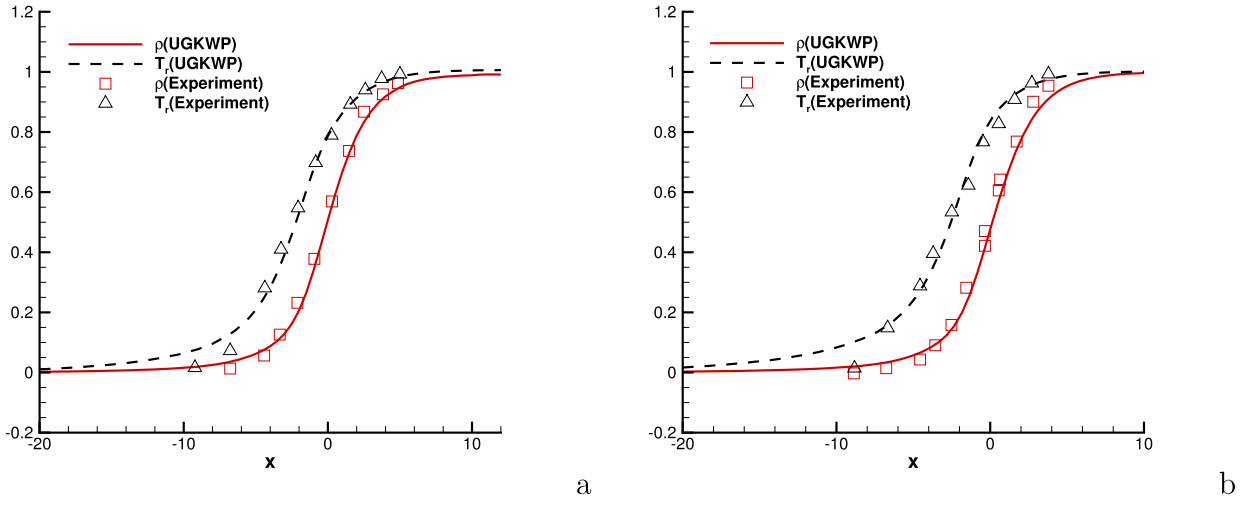

Fig. 6. Normalized density and rotational temperature profile of normal shock wave at M = 7 (left) and M = 12.9 (right). The experiment results are shown in symbol, and the UGKWP solution are shown in line. x is normalized by the mean free path based on the sonic temperature.

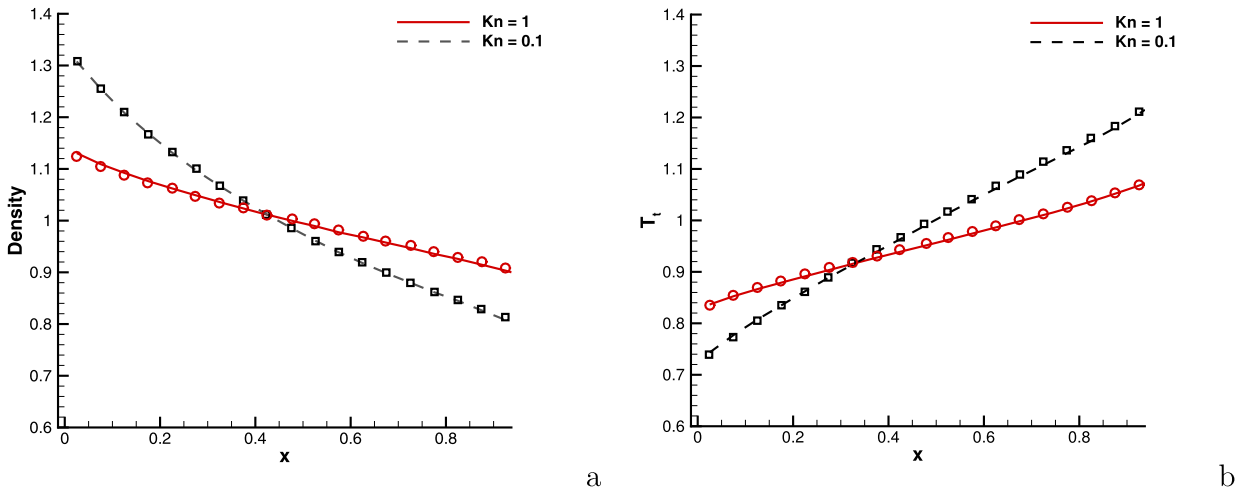

Fig. 7. (a) Density and (b) translational temperature profile of planar Fourier flow at $Kn = 0.1$ (square) and $Kn = 1$ (circle). The DSMC results are shown in symbol, and the UGKWP solution are shown in line.

Table 1
Comparison of the computational cost between UGKWP method and the implicit UGKS in a 48 cores workstation.

M_∞	Kn_∞	Time of Implicit UGKS	Time of UGKWP (Nitrogen)	Time ratio $\frac{\text{UGKS}}{\text{UGKWP}}$
4.25	0.121	265.6 hours	32 hours	8.3
4.25	0.031	265.6 hours	3.1 hours	85.7

$$\mu = \mu_{ref}(T_t)^{2/3}\phi(B)/\phi(BT_t),$$
$$Z_{rot}(T_t, T_r) = \frac{3}{4}\pi \frac{\phi(BT_t)}{(BT_t)^{1/6}} \frac{9BT_t}{BT_t + 8}\left(\frac{T_r}{T_t}\right)\left[0.461 + 0.5581\left(\frac{T_r}{T_t}\right) + 0.0358\left(\frac{T_r}{T_t}\right)^2\right], \tag{47}$$
$$\phi(t) = 0.767 + 0.233t^{-1/6}\exp\{-1.17(t-1)\},$$

with the rotational characteristic parameter $B = 0.34$, and the reference viscosity is calculated by the hard sphere model,

$$\mu_{ref} = \frac{5\sqrt{\pi}}{16}\text{Kn}. \tag{48}$$

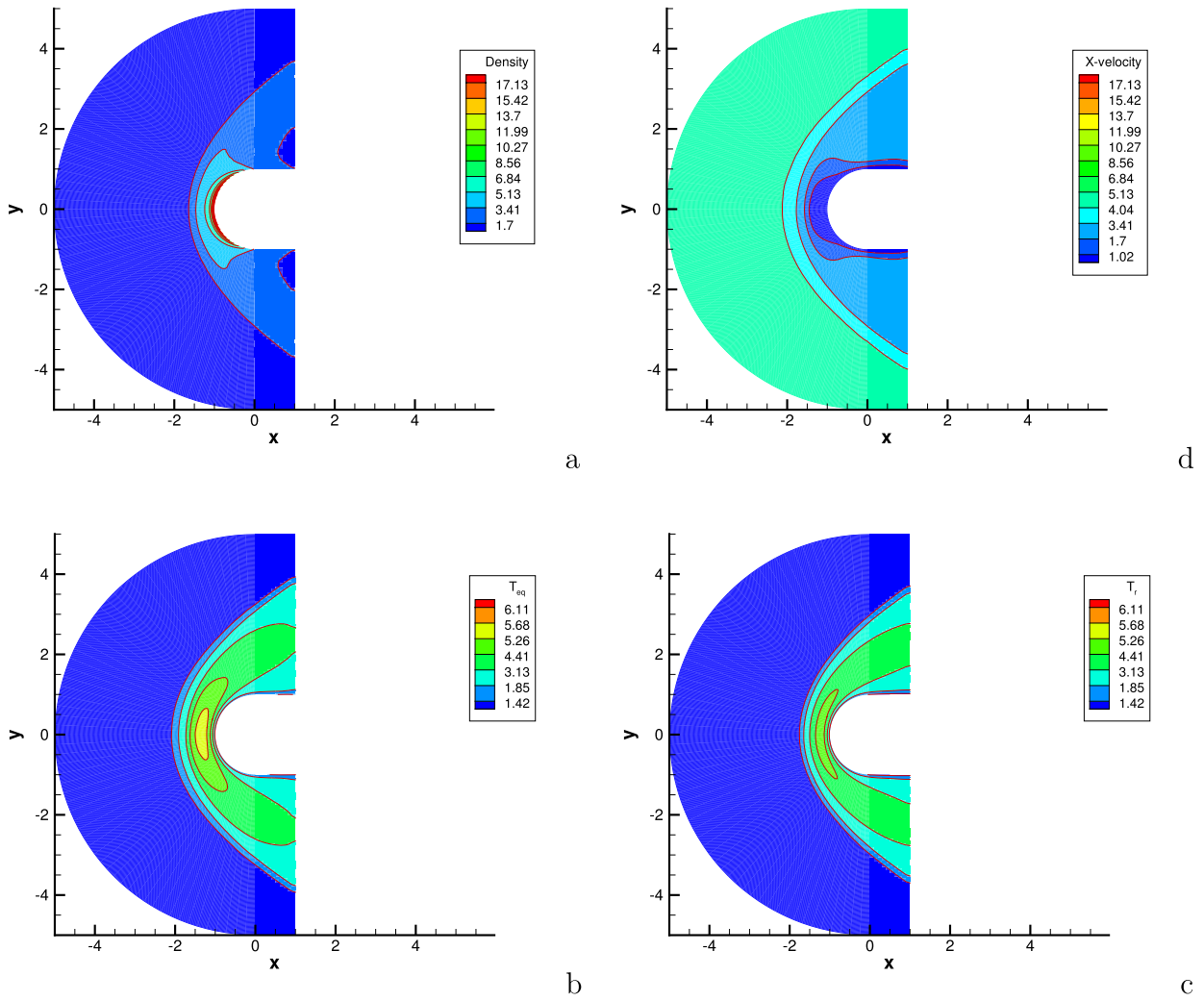

Fig. 8. (a) Density and (b) x direction velocity (c) temperature (d) rotational temperature contour for $Kn = 0.1$ and $M = 5.0$. (For interpretation of the colours in the figure(s), the reader is referred to the web version of this article.)

Table 2
Comparison of the drag coefficients.

M_∞	Kn_∞	Experiment (Air)	UGKWP (Nitrogen)		UGKS (Nitrogen)	
			Drag coefficient	Relative error	Drag coefficient	Relative error
4.25	0.121	1.69	1.636 ± 0.0005	$-3.21\% \pm 0.03\%$	1.694	-0.27%
4.25	0.031	1.35	1.346 ± 0.0007	$-0.25\% \pm 0.05\%$	1.355	-0.39%
10	0.01	-	1.215 ± 0.0001	-	-	-

The Knudsen numbers are set as $Kn = 1.0, 0.1, 0.01, 0.001$, and the cell size and the time step are fixed as $\Delta x = 0.005$ and $\Delta t = 0.001912$. These four test cases are calculated up to $t = 0.1912$. As shown in Fig. 4, in the rarefied regime when $Kn = 1.0$, the difference between the translational temperature and the rotational temperature is obvious, which shows a highly non-equilibrium effect. With the decrease of the Knudsen number, these two temperatures tend to the same. From the figures, we can see that the UGKWP solutions agree well with the reference solutions [37] in the first three cases. In the continuum case when $Kn = 0.001$, the UGKWP solution is slightly more diffusive than the reference solution which is calculated by a high order scheme.

4.3. Normal shock

To demonstrate the accuracy of UGKWP method in capturing the highly non-equilibrium flow, the one dimensional shock wave is studied. For the nitrogen gas, the viscous coefficient is given as

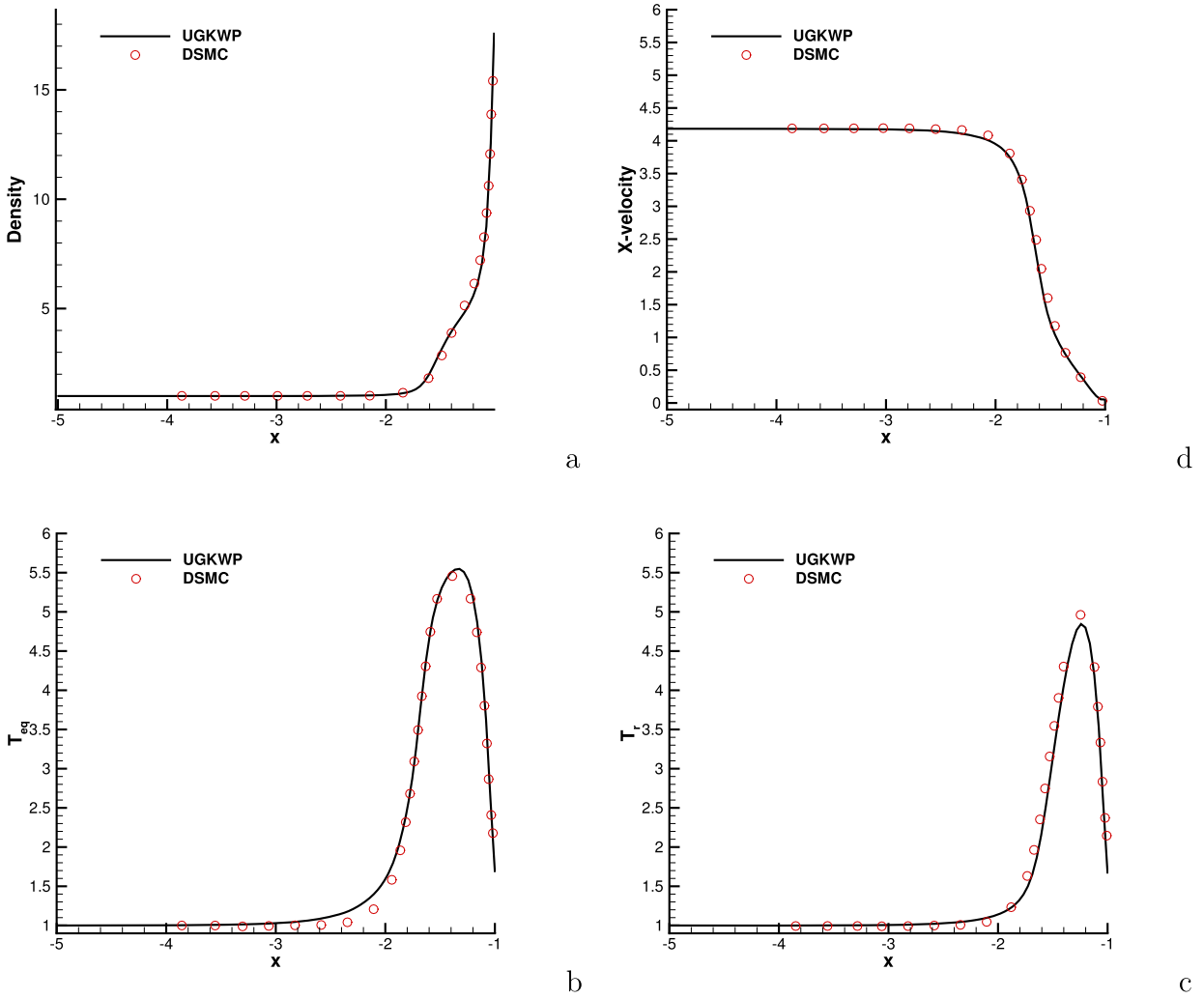

Fig. 9. (a) Density, (b) x direction velocity, (c) temperature, (d) rotational temperature profile along stagnation line for M = 5.0 and Kn = 0.1. The DSMC results are shown in symbol, and the UGKWP solutions are shown in line.

$$\mu = \mu_{ref} \left(\frac{T}{T_0} \right)^{\omega}, \tag{49}$$

with the temperature dependency index $\omega = 0.72$, and the reference viscosity

$$\mu_{ref} = \frac{15\sqrt{\pi}}{2(5-2\omega)(7-2\omega)} \mathrm{Kn}. \tag{50}$$

In this calculation, the reference length is the upstream mean free path, and the computational domain is [-25,25] with 100 cells. The upstream ($x \leq 0$) and downstream ($x > 0$) is connected by the Rankine-Hugoniot condition. The collision rotation number used in the UGKWP is $Z_{rot} = 2.4$. In order to reduce the statistical noise, 5×10^3 simulation particles are used in each cell. The normalized temperature and density from UGKWP and DSMC [21] at M = 1.53, 4.0, 5.0, 7.0 are plotted in Fig. 5. As analyzed before, since the Rykov model reduces to Shakhov model at large Z_{rot}, the early rising of the temperature occurs at high Mach number. The reason for the early rising of temperature is due to the use of the single relaxation time in these kinetic models, which is inconsistent with the physical reality that the high speed particles should have shorter relaxation time. By a simple control on the relaxation time of the high particles, one can get significant improvement on the problem of early rising of the temperature [38].

Next we compare UGKWP results with experiment data for nitrogen shock waves with upstream Mach number M = 7 and M = 12.9. The rotational collision number is given by

$$Z_{rot} = \frac{Z_{rot}^{\infty}}{1 + (\pi^2/2)\sqrt{T^*/T_t} + (\pi^2/4 + \pi)(T^*/T_t)}, \tag{51}$$

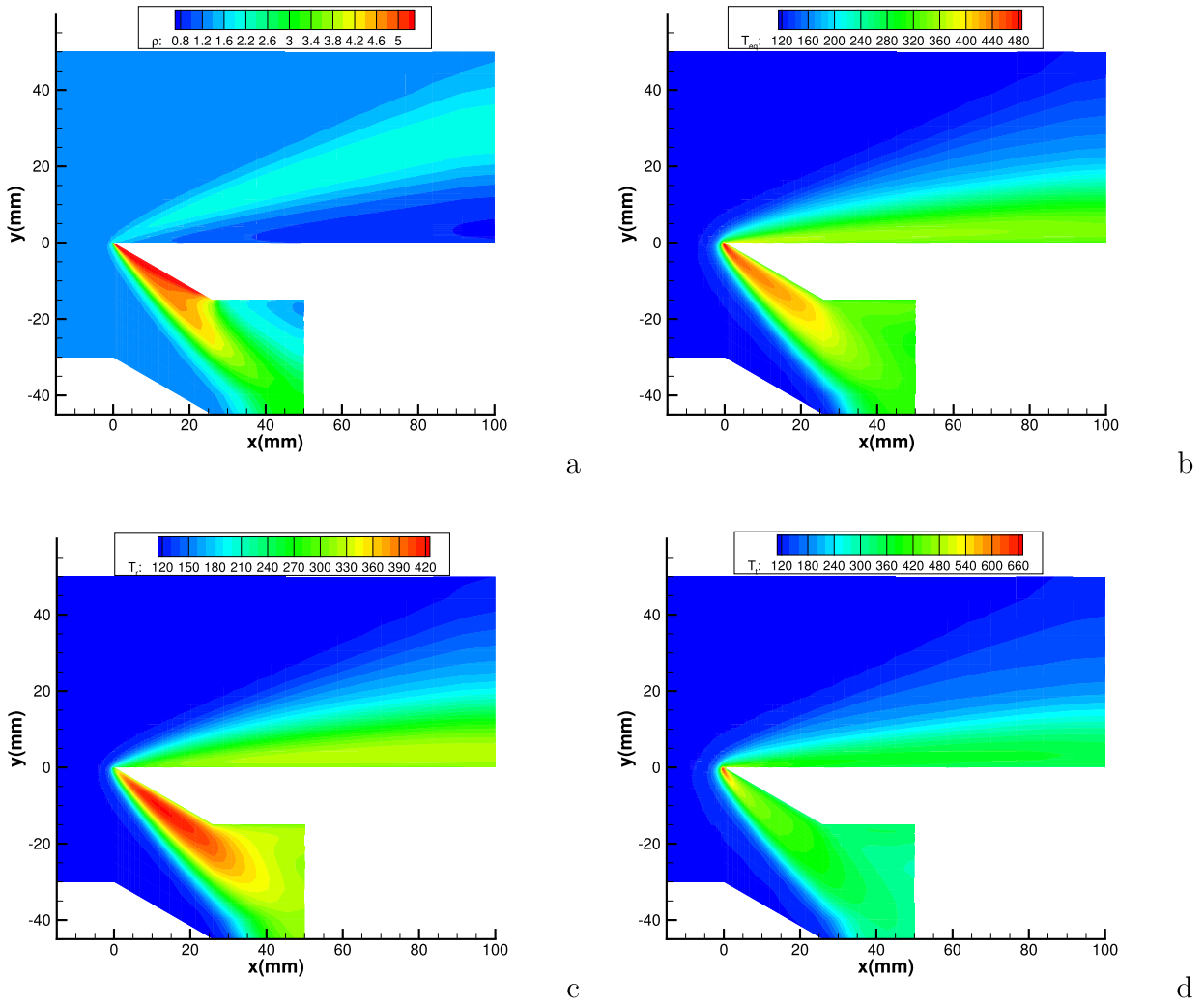

Fig. 10. (a) Density and (b) temperature (c) rotational temperature (d) translational temperature contour for the hypersonic flow passing a flat plate.

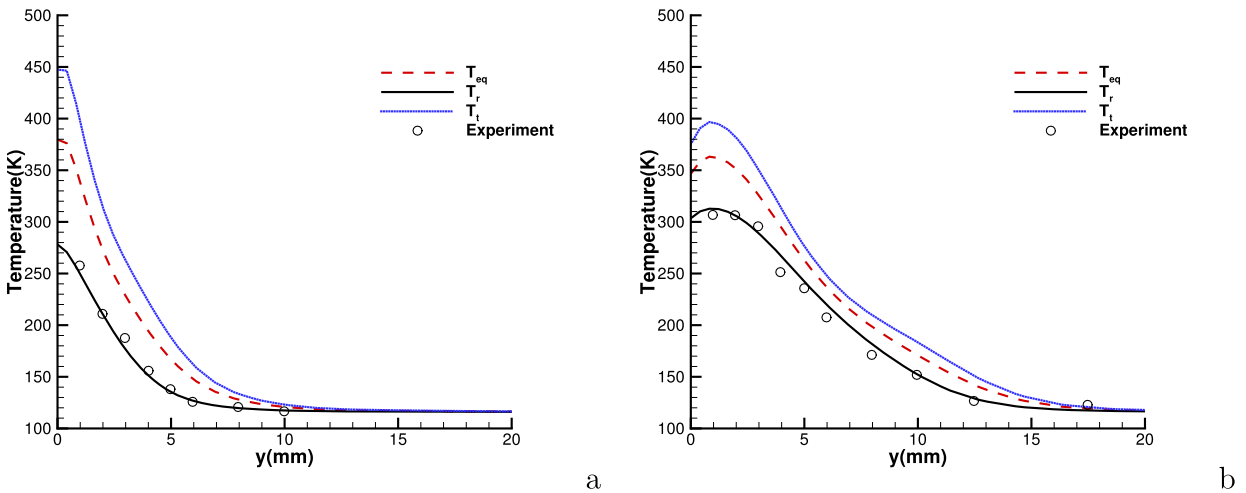

Fig. 11. Temperature profiles along vertical lines at (a) x = 5 mm and (b) x = 20 mm. The experiment results [41] are shown in symbol, and the UGKWP solutions are shown in line.

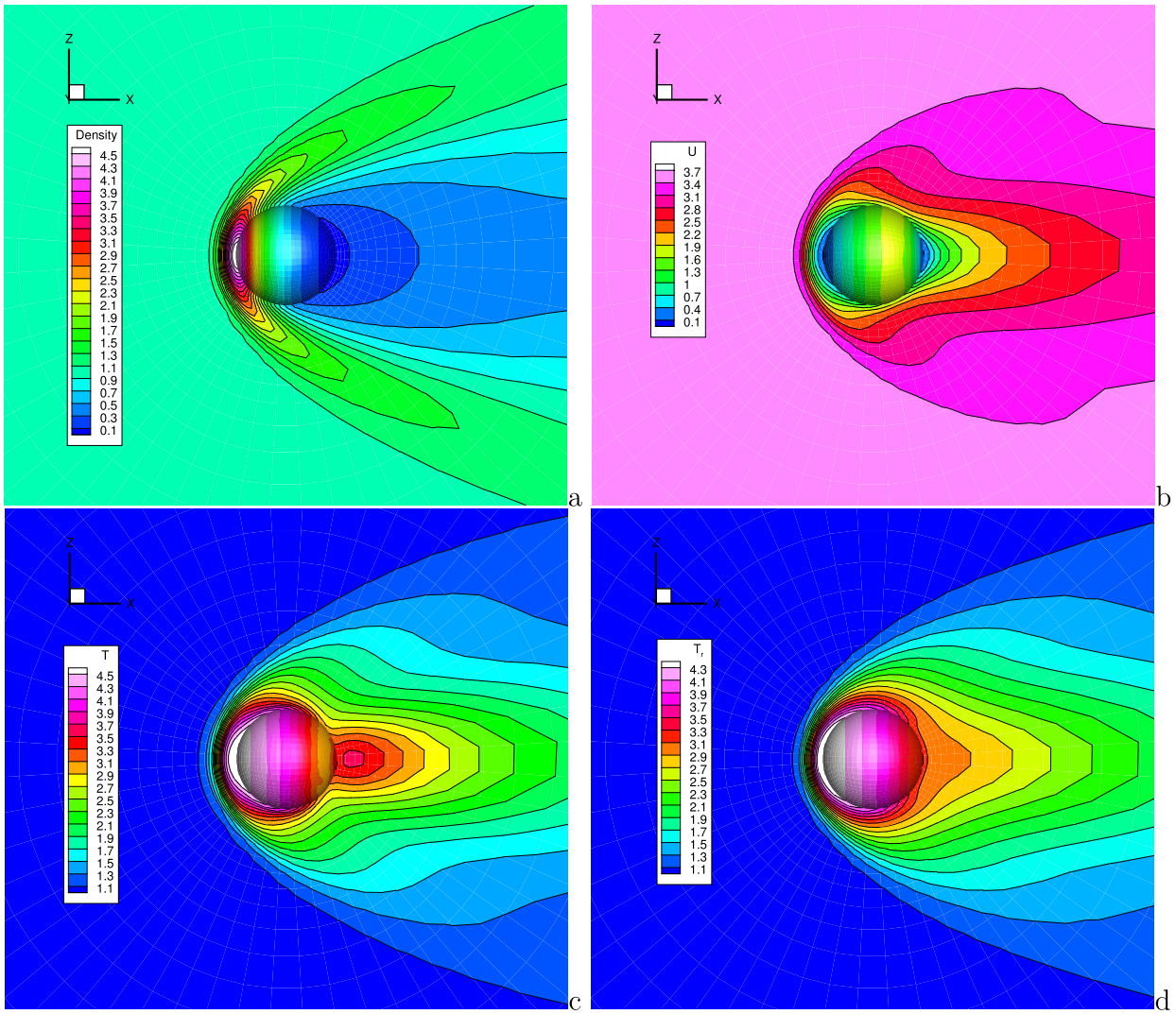

Fig. 12. (a) Density and (b) x direction velocity (c) temperature (d) rotational temperature contour for $Kn = 0.031$ and $\mathrm{M} = 4.25$.

where $Z_{rot}^{\infty} = 18.0$ and $T^* = 91.5K$ are used in the computation. Fig. 6 shows the reasonable agreement with the experimental data [39].

4.4. Planar Fourier flow

In this case, we consider the flow driven by the temperature gradient. Consider the nitrogen gas between two parallel plates with a distance L. The temperatures at the bottom and top are fixed with values $T_0 = 4/3$ and $T_1 = 2/3$. We set up the simulation as a 1D problem in the x-direction. The computational domain is [0,1] with 20 cells and each cell has a maximum number of 150 particles. The initial density and Mach number of the gas inside the channel are 1 and 0. Diffuse boundary conditions are adopted at both plates. Fig. 7 shows the density and translational temperature computed by UGKWP, which are in good agreement with the DSMC results [40].

4.5. Flow around a blunt circular cylinder

Next we calculate the hypersonic nitrogen gas flow passing over a blunt circular cylinder at Mach number $\mathrm{M} = 5.0$ and Knudsen number $\mathrm{Kn} = 0.1$. The cylinder has a radius $R = 0.01m$ and the computational domain is divided with 64×150 cells. For nitrogen gas, the molecular number density n is $n = 1.2944 \times 10^{21}$ /m^3. The viscosity coefficient at upstream is $\mu = 1.65788 \times 10^{-5}$ Ns/m^2. The cylinder has a surface with constant temperature $T_w = 273$ K, and diffusive boundary condition is adopted here. The rotational collision number Z_{rot} is calculated by Eq. (51). The dimensionless quantities are used with respect to the reference length as the cylinder radius $L_{ref} = R$, the reference velocity $U_{ref} = \sqrt{2RT_{\infty}}$, the reference time

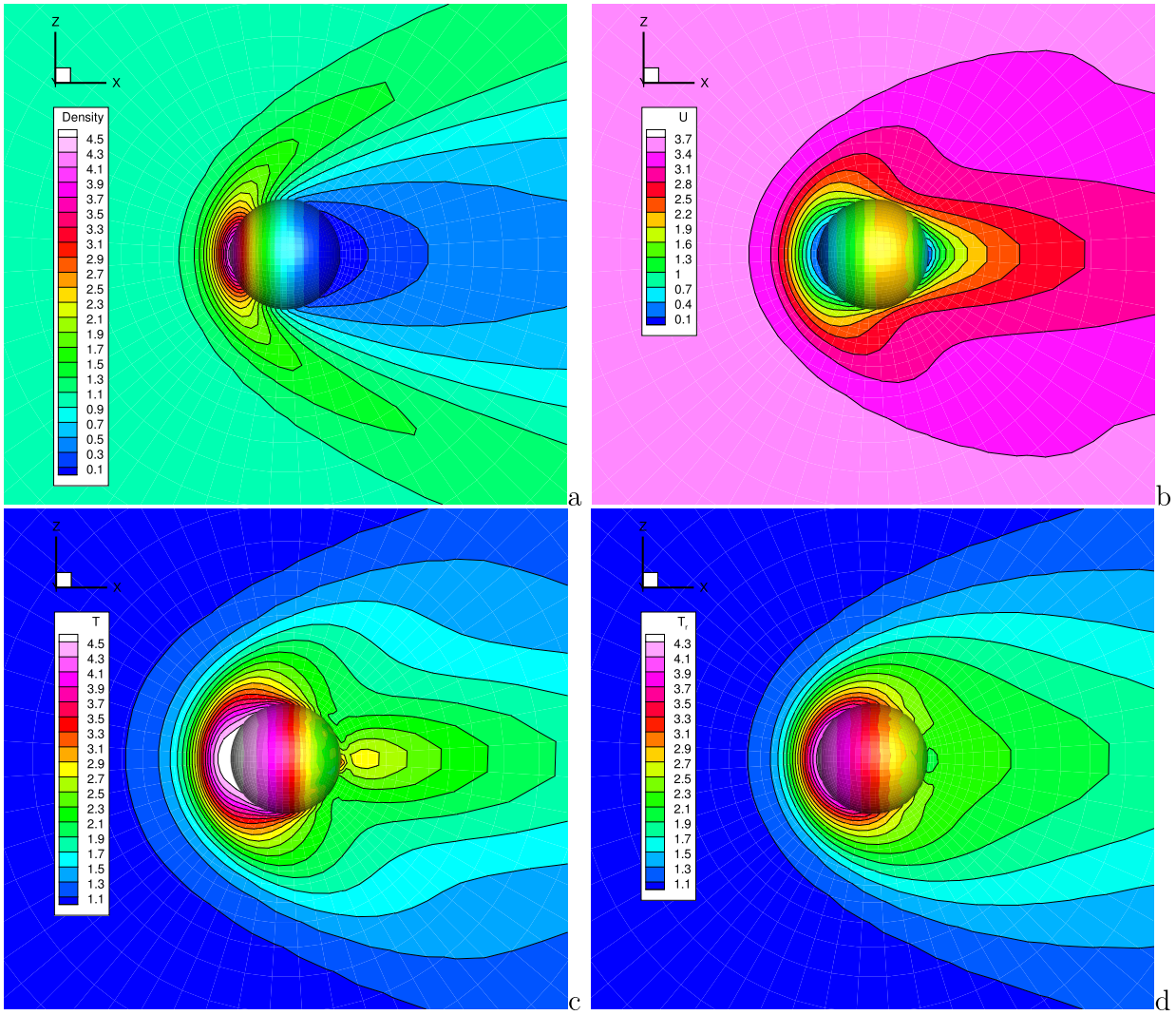

Fig. 13. (a) Density and (b) x direction velocity (c) temperature (d) rotational temperature contour for $Kn = 0.121$ and $M = 4.25$.

$t_{ref} = L_{ref}/U_{ref}$, the reference density $\rho_{ref} = \rho_\infty$, and the reference temperature $T_{ref} = T_\infty$. The distribution of density, velocity, temperature, and rotational temperature are shown in Fig. 8. Fig. 9 shows the comparisons between UGKWP results and DSMC solutions [21]. Reasonable agreement have been achieved.

4.6. Flow passing a flat plate

Following the experiment conducted by Tsuboi and Matsumoto [41], we simulate the hypersonic rarefied gas flow over a flat plate using UGKWP for nitrogen gas. The case is run 34, where the nozzle exit Mach number is $M = 4.89$, the nozzle exit pressure is $P_e = 2.12$ Pa, the stagnation pressure is $P_0 = 983$ Pa and the nozzle exit temperature is $T_e = 116$K. The stagnation temperature is $T_0 = 670$K, which is used as a reference temperature to determine the viscosity coefficient,

$$\mu = \mu_{ref} \left(\frac{T_t}{T_0} \right)^{\omega}.$$

The reference viscosity is defined as

$$\mu_{ref} = \frac{5\sqrt{2\pi RT_{ref}}}{16} \rho_{ref} l_{mfp},$$

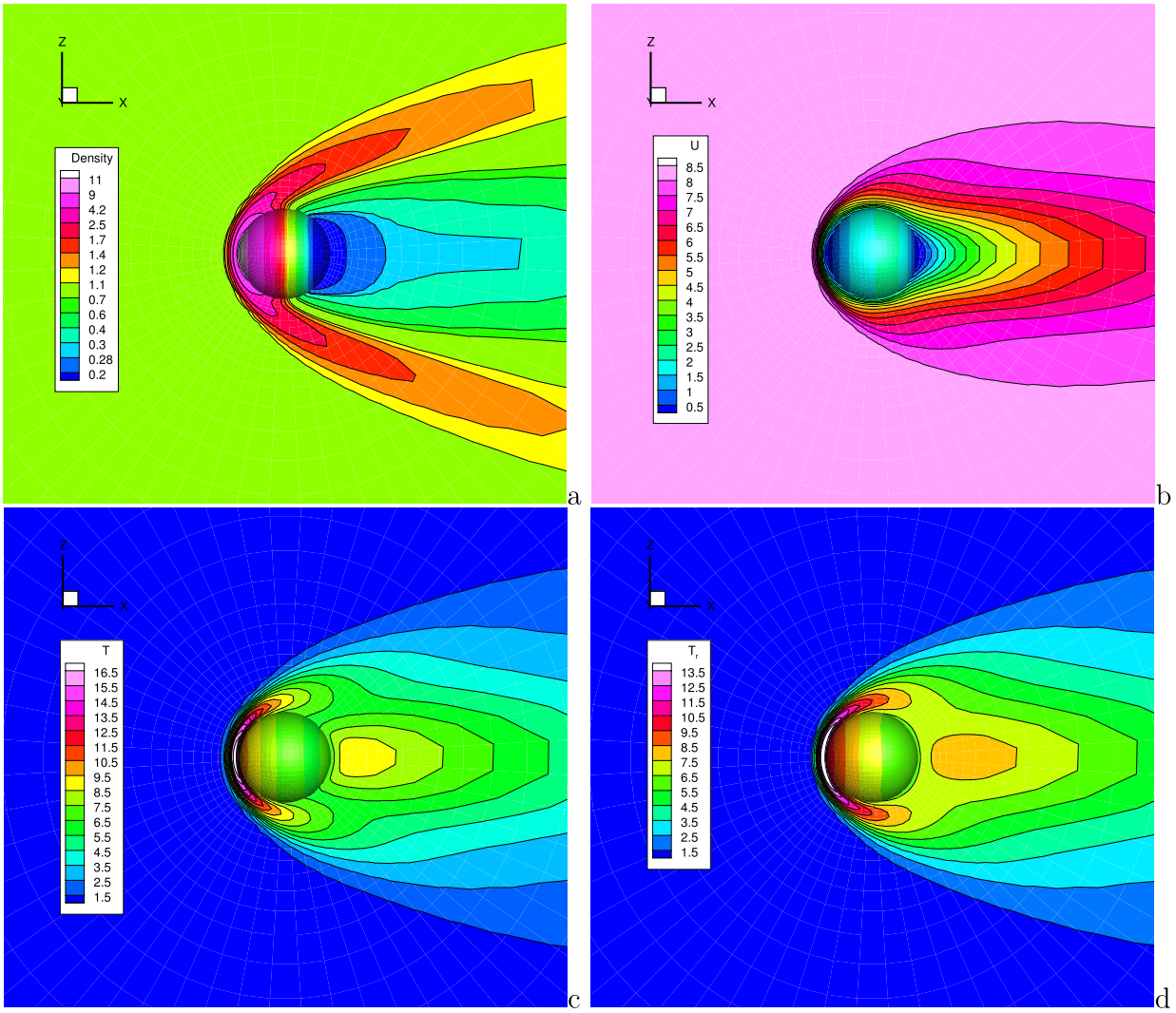

Fig. 14. (a) Density and (b) x direction velocity (c) temperature (d) rotational temperature contour for $Kn = 0.01$ and $M = 10$.

where $\rho_{ref} = 6.15 \times 10^{-5}$ kg m $^{-3}$ is the reference density, $l_{mfp} = 0.78mm$ is the mean free path and $T_{ref} = 116$ K is the reference temperature. The flat plate has a constant wall temperature of 290 K and the diffusive boundary condition is adopted at the plate. In this case, the relaxation collision number Z_{rot} is set to be 3.5.

In this study, 59×39 grid points are used above the plate and 44×25 grid points are used below the plate, which has the same configuration as that used in UGKS [21]. The contours of the density, equilibrium temperature, rotational temperature and translational temperature are shown in Fig. 10. The temperature distribution along the vertical line above the flat plate at $x = 5$ mm and $x = 20$ mm are shown in Fig. 11, which show good agreement with the experiment measurements.

4.7. Flow passing a sphere

The three dimensional case is about $M = 4.25$ nitrogen gas flow passing through a sphere at $Kn = 0.031$ and $Kn = 0.121$ in the transition regime. The radius of sphere is 10^{-3} m and the surface mesh of the sphere is divided into 6 blocks with 16×16 mesh points in each block with a minimum surface spacing 6.255×10^{-5} m. Diffusive wall boundary condition with a constant temperature $T_w = 302$ K is imposed on the surface. The computational domain is composed of 29700 hexahedra with growth rate 1.1 and smallest cell height 5×10^{-5} m. The inflow is diatomic nitrogen gas with molecular mass $m = 4.65 \times 10^{-26}$ kg and diameter $d = 4.17 \times 10^{-10}$ m. The upstream flow temperature is set to be $T_\infty = 65$ K. The reference viscosity is given by the variable hard sphere (VHS) model with $\omega = 0.74$. For the case of $Kn = 0.031$, the time-averaging starts from 2500 steps and continues for 13000 steps with an initial field computed by 1000 steps from GKS. The total computation takes 13500 time steps, and runs on a workstation with (Dual CPU) Intel Xeon Platinum 8168 at 2.70 GHz with 48 cores. The distribution of density, velocity, temperature, and rotational temperature are shown in Fig. 12.

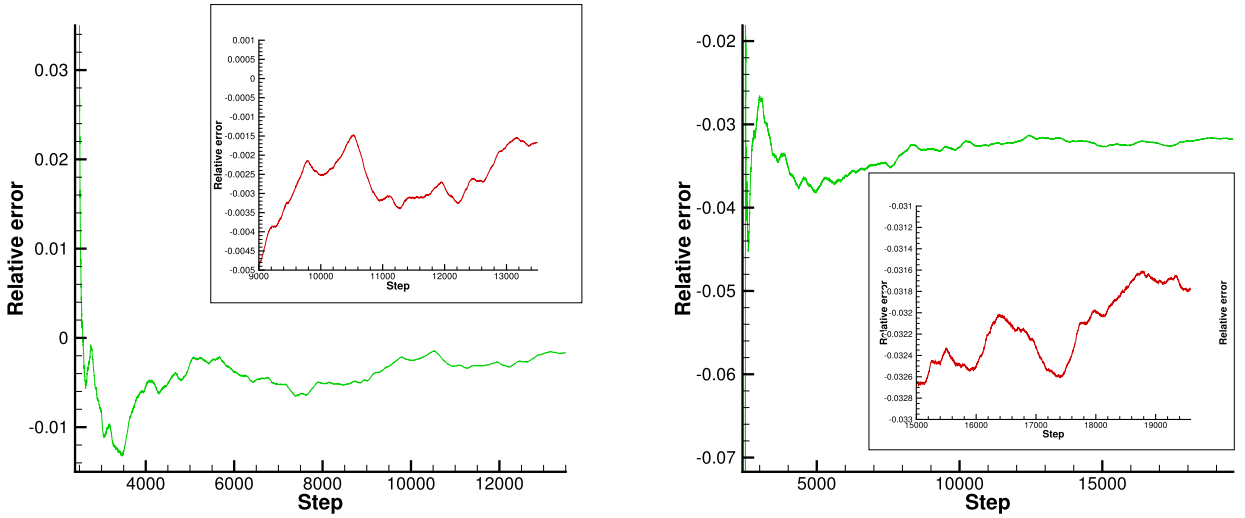

Fig. 15. Relative error of the drag coefficient at $Kn = 0.031$ (left) and $Kn = 0.121$ (right).

For the case of Kn = 0.121, the time-averaging starts from 2500 steps and continues for 17000 steps with an initial field computed by 1000 steps from GKS. The distribution of density, velocity, temperature, and rotational temperature are shown in Fig. 13. Fig. 15 shows the relative error with drag coefficient (Air) given by experiment [42]. Both UGKS and UGKWP can obtain satisfactory drag coefficients compared with the experimental data. However, the computational efficiency is greatly improved by the UGKWP method. The detail comparison of the computational cost between the UGKWP method and the implicit UGKS [43] is shown in Table 1. Apart from the above two cases, we also compute a hypersonic case with M = 10 and Kn = 0.01. In order to calculate this hypersonic case, the computational cost for the UGKS will become unaffordable since it needs a huge discrete velocity space to get an accurate solution. For the UGKWP method, the computation for Mach 10 case needs only 1.46 hour with a personal 48 cores workstation. The distribution of density, velocity, temperature, and rotational temperature are shown in Fig. 14. The drag coefficient is also shown in Table 2.

5. Conclusion

In this paper, the unified gas-kinetic wave-particle method has been developed for diatomic gas, where the Rykov model is used for the molecular collision term with the exchange of translational and rotational energy. Based on the direct modelling, the UGKWP constructs the discrete governing equations according to the cell's Knudsen number and computes gas dynamic solution in all flow regimes with a unified approach. Instead of the DVM discretization in the UGKS, the gas distribution function in UGKWP is composed of the contribution from the particle and wave, where analytical solution can be obtained for the wave part. At the same time, the weights for distributing particle and wave are related to the cell Knudsen number through $\exp(-\Delta t/\tau)\rho$ and $(1-\exp(-\Delta t/\tau))\rho$. As a result, the UGKWP becomes a particle method in the highly rarefied regime $\Delta t \leq \tau$, and becomes a macroscopic NS solver in the continuum flow regime $\Delta t \gg \tau$. There is a smooth dynamic transition between different regimes in UGKWP. Therefore, besides asymptotic property to the NS solver, the UGKWP has multiple efficiency preserving property for a multiscale flow problem, where the most efficient approach is used in the corresponding regime, such as the hypersonic flow passing through a flying vehicle in near space with 5 to 6 orders of magnitude difference in the local Knudsen number. The calculation for a 3D problem at high speed and different Knudsen numbers can be conducted by UGKWP with a personal computer. The UGKWP for diatomic gas has been validated in many test cases. Reasonable agreements have been obtained among UGKWP solutions, DSMC results, and experimental measurements. In the future, the UGKWP will be further developed with the inclusion of vibrational mode and partially ionization [30].

Declaration of competing interest

The authors declare that they have no known competing financial interests or personal relationships that could have appeared to influence the work reported in this paper.

Acknowledgements

The authors would like to thank reviewers for their constructive comment. The current research is supported by National Numerical Windtunnel project and National Science Foundation of China 11772281, 91852114.

References

[1] P. Bhatnagar, E. Gross, M. Krook, A model for collision processes in gases. I. Small amplitude processes in charged and neutral one-component systems, Phys. Rev. 94 (3) (1954) 511–525.
[2] L.H. Holway Jr, New statistical models for kinetic theory: methods of construction, Phys. Fluids 9 (9) (1966) 1658–1673.
[3] E. Shakhov, Generalization of the Krook kinetic relaxation equation, Fluid Dyn. 3 (5) (1968) 95–96.
[4] G. Bird, Approach to translational equilibrium in a rigid sphere gas, Phys. Fluids 6 (10) (1963) 1518–1519.
[5] C. Chu, Kinetic theoretic description of the formation of a shock wave, Phys. Fluids 8 (1) (1965) 12–22.
[6] J. Yang, J. Huang, Rarefied flow computations using nonlinear model Boltzmann equations, J. Comput. Phys. 120 (2) (1995) 323–339.
[7] L. Mieussens, Discrete-velocity models and numerical schemes for the Boltzmann-BGK equation in plane and axisymmetric geometries, J. Comput. Phys. 162 (2) (2000) 429–466.
[8] F. Tcheremissine, Direct numerical solution of the Boltzmann equation, Tech. Rep., DTIC Document, 2005.
[9] V. Kolobov, R. Arslanbekov, V. Aristov, A. Frolova, S. Zabelok, Unified solver for rarefied and continuum flows with adaptive mesh and algorithm refinement, J. Comput. Phys. 223 (2) (2007) 589–608.
[10] Z. Li, H. Zhang, Gas-kinetic numerical studies of three-dimensional complex flows on spacecraft re-entry, J. Comput. Phys. 228 (4) (2009) 1116–1138.
[11] K. Xu, J.-C. Huang, A unified gas-kinetic scheme for continuum and rarefied flows, J. Comput. Phys. 229 (20) (2010) 7747–7764.
[12] L. Wu, J. Zhang, J.M. Reese, Y. Zhang, A fast spectral method for the Boltzmann equation for monatomic gas mixtures, J. Comput. Phys. 298 (2015) 602–621.
[13] V.V. Aristov, Direct Methods for Solving the Boltzmann Equation and Study of Nonequilibrium Flows, vol. 60, Springer Science & Business Media, 2012.
[14] S. Jin, Efficient asymptotic-preserving (AP) schemes for some multiscale kinetic equations, SIAM J. Sci. Comput. 21 (2) (1999) 441–454.
[15] B. Dubroca, L. Mieussens, A conservative and entropic discrete-velocity model for rarefied polyatomic gases, in: ESAIM: Proceedings, in: EDP Sciences, vol. 10, 2001, pp. 127–139.
[16] R. Chen, R. Agarwal, F. Tcheremissine, Computation of Hypersonic Flow of a Diatomic Gas in Rotational Nonequilibrium Past a Blunt Body Using the Generalized Boltzmann Equation, AIP Conference Proceedings, vol. 1084, American Institute of Physics, 2008, pp. 476–482.
[17] K. Xu, Direct Modeling for Computational Fluid Dynamics: Construction and Application of Unified Gas-Kinetic Scheme, World Scientic, 2015.
[18] J.-C. Huang, K. Xu, P. Yu, A unified gas-kinetic scheme for continuum and rarefied flows II: multi-dimensional cases, Commun. Comput. Phys. 12 (3) (2012) 662–690.
[19] C. Liu, K. Xu, Q. Sun, Q. Cai, A unified gas-kinetic scheme for continuum and rarefied flows IV: Full Boltzmann and model equations, J. Comput. Phys. 314 (2016) 305–340.
[20] Z. Wang, H. Yan, Q. Li, K. Xu, Unified gas-kinetic scheme for diatomic molecular flow with translational, rotational, and vibrational modes, J. Comput. Phys. 350 (2017) 237–259.
[21] S. Liu, P. Yu, K. Xu, C. Zhong, Unified gas-kinetic scheme for diatomic molecular simulations in all flow regimes, J. Comput. Phys. 259 (2014) 96–113.
[22] Z. Guo, J. Li, K. Xu, On unified preserving properties of kinetic schemes, arXiv preprint, arXiv:1909.04923, 2019.
[23] Y. Zhu, C. Zhong, K. Xu, Implicit unified gas-kinetic scheme for steady state solutions in all flow regimes, J. Comput. Phys. 315 (2016) 16–38.
[24] Y. Zhu, C. Zhong, K. Xu, Unified gas-kinetic scheme with multigrid convergence for rarefied flow study, Phys. Fluids 29 (9) (2017) 096102.
[25] Y. Zhu, C. Zhong, K. Xu, An implicit unified gas-kinetic scheme for unsteady flow in all Knudsen regimes, J. Comput. Phys. 386 (2019) 190–217.
[26] C. Liu, Y. Zhu, K. Xu, Unified gas-kinetic wave-particle methods I: Continuum and rarefied gas flow, J. Comput. Phys. 401 (2020) 108977.
[27] Y. Zhu, C. Liu, C. Zhong, K. Xu, Unified gas-kinetic wave-particle methods. II. Multiscale simulation on unstructured mesh, Phys. Fluids 31 (6) (2019) 067105.
[28] K. Xu, A gas-kinetic BGK scheme for the Navier–Stokes equations and its connection with artificial dissipation and Godunov method, J. Comput. Phys. 171 (1) (2001) 289–335.
[29] W. Li, C. Liu, Y. Zhu, J. Zhang, K. Xu, Unified gas-kinetic wave-particle methods III: Multiscale photon transport, J. Comput. Phys. 408 (2020) 109280.
[30] C. Liu, K. Xu, Unified gas-kinetic wave-particle methods IV: Multi-species gas mixture and plasma transport, Adv. Aerodyn. 3 (2021) 9.
[31] K. Xu, X. He, C. Cai, Multiple temperature kinetic model and gas-kinetic method for hypersonic non-equilibrium flow computations, J. Comput. Phys. 227 (14) (2008) 6779–6794.
[32] S. Chapman, T.G. Cowling, D. Burnett, The Mathematical Theory of Non-uniform Gases: An Account of the Kinetic Theory of Viscosity, Thermal Conduction and Diffusion in Gases, Cambridge University Press, 1990.
[33] G. May, B. Srinivasan, A. Jameson, An improved gas-kinetic BGK finite-volume method for three-dimensional transonic flow, J. Comput. Phys. 220 (2) (2007) 856–878.
[34] V. Rykov, V. Skobelkin, Macroscopic description of the motions of a gas with rotational degrees of freedom, Fluid Dyn. 13 (1) (1978) 144–147.
[35] G. Bird, Molecular Gas Dynamics and the Direct Simulation Monte Carlo of Gas Flows, vol. 508, Clarendon, Oxford, 1994, p. 128.
[36] V. Rykov, V. Titarev, E. Shakhov, Shock wave structure in a diatomic gas based on a kinetic model, Fluid Dyn. 43 (2) (2008) 316–326.
[37] J. Wu, Z. Li, X. Jiang, One-dimensional shock-tube and two-dimensional plate flows in Boltzmann-Rykov model involving rotational energy, Chin. J. Comput. Phys. 30 (3) (2013) 326–336.
[38] X. Xu, Y. Chen, K. Xu, Modeling and computation for non-equilibrium gas dynamics: beyond single relaxation time kinetic models, Phys. Fluids 33 (1) (2021) 011703.
[39] F. Robben, L. Talbot, Experimental study of the rotational distribution function of nitrogen in a shock wave, Phys. Fluids 9 (4) (1966) 653–662.
[40] L. Wu, C. White, T.J. Scanlon, J.M. Reese, Y. Zhang, A kinetic model of the Boltzmann equation for non-vibrating polyatomic gases, J. Fluid Mech. 763 (2015) 24–50.
[41] N. Tsuboi, Y. Matsumoto, Experimental and numerical study of hypersonic rarefied gas flow over flat plates, AIAA J. 43 (6) (2005) 1243–1255.
[42] J. Wendt, Drag coefficients of spheres in hypersonic non-continuum flow, Tech. Rep. AD739250, von Karman Institute for Fluid Dynamics, 1971.
[43] D. Jiang, M. Mao, J. Li, X. Deng, An implicit parallel UGKS solver for flows covering various regimes, Adv. Aerodyn. 1 (1) (2019) 8.